RECENT SOVIET DEVELOPMENTS IN SEISMOLOGY

M. Ness

Informatics, Incorporated

Prepared for:

Navy Foreign Language Service
Defense Advanced Research Projects Agency

8 May 1975

UNCLASSIFIED

SECURITY CLASSIFICATION OF THIS PAGE (When Data Entered)

REPORT DOCUMENTATION PAGE		READ INSTRUCTIONS BEFORE COMPLETING FORM
1. REPORT NUMBER	2. GOVT ACCESSION NO.	3. RECIPIENT'S CATALOG NUMBER AD-A009 817
4. TITLE (and Subtitle) Recent Soviet Developments in Seismology		5. TYPE OF REPORT & PERIOD COVERED Scientific . . . Interim
		6. PERFORMING ORG. REPORT NUMBER
7. AUTHOR(s) M. Ness		8. CONTRACT OR GRANT NUMBER(s) N00600-75-C-0018
9. PERFORMING ORGANIZATION NAME AND ADDRESS Informatics Inc. 6000 Executive Boulevard Rockville, Maryland 20852		10. PROGRAM ELEMENT, PROJECT, TASK AREA & WORK UNIT NUMBERS DARPA Order No. 2790 Program Code No. L13003
11. CONTROLLING OFFICE NAME AND ADDRESS Defense Advance Research Projects Agency/TAO 1400 Wilson Boulevard Arlington, Virginia 22209		12. REPORT DATE May 8, 1975
		13. NUMBER OF PAGES 74
14. MONITORING AGENCY NAME & ADDRESS(if different from Controlling Office) U. S. Navy Foreign Language Service 4301 Suitland Road, Bldg. 5 Washington, D. C. 20390		15. SECURITY CLASS. (of this report) UNCLASSIFIED
		15a. DECLASSIFICATION/DOWNGRADING SCHEDULE

16. DISTRIBUTION STATEMENT (of this Report)

Approved for public release; distribution unlimited.

17. DISTRIBUTION STATEMENT (of the abstract entered in Block 20, if different from Report)

18. SUPPLEMENTARY NOTES

Scientific . . . Interim

19. KEY WORDS (Continue on reverse side if necessary and identify by block number)

seismology	seismometer
computer seismology	seismograph
explosion seismology	seismic recording system
seismological observatory	nuclear explosion

20. ABSTRACT (Continue on reverse side if necessary and identify by block number)

The present compilation of abstracts contains recent information on seismometry, computer seismology, explosion seismology, and general information on seismology, including some material on the Rumanian seismological stations and several articles on seismological research in Communist China.

DD FORM 1 JAN 73 1473 EDI

UNCLASSIFIED

SECURITY CLASSIFICATION OF THIS PAGE (When Data Entered)

RECENT SOVIET DEVELOPMENTS IN SEISMOLOGY

Sponsored by

Defense Advanced
Research Projects Agency

DARPA Order No. 2790

May 8, 1975

ARPA Order No. 2790
Program Code No. L13003
Name of Contractor:
Informatics Inc.
Effective Date of Contract:
July 1, 1974
Contract Expiration Date:
June 30, 1975
Amount of Contract: $306,023

Contract No. N00600-75-C-0018
Principal Investigator:
Stuart C. Hibben
Tel: (301) 770-3000
Program Manager:
Klaus Liebhold
Tel: (301) 770-3000
Short Title of Work:
Soviet seismology

This research was supported by the Defense Advanced Research Projects Agency and was monitored by the U. S. Navy Foreign Language Service under Contract No. N00600-75-C-0018. The publication of this report does not constitute approval by any government organization or Informatics Inc. of the inferences, findings, and conclusions contained herein. It is published solely for the exchange and stimulation of ideas.

informatics inc
Systems and Services Company
6000 Executive Boulevard
Rockville, Maryland 20852
(301) 770-3000 Telex: 89 521

FOREWORD

The present compilation of abstracts contains recent information on seismometry, computer seismology, explosion seismology, and general information on seismology, including some material on the Rumanian seismological stations and several articles on seismological research in Communist China.

TABLE OF CONTENTS

1. Seismometry

Aranovich, Z. I., and O. Ye. Starovoyt. Status of observations with the SD-1 long-period seismograph in the USSR. Fizika Zemli, no. 1, 1975, 88-94.

The introduction of SD-1 seismographs into base stations of the Unified System of Seismic Observations was initiated in 1968 as part of studies of the upper mantle in Europe from observations of long-period seismographs. The planned network of stations equipped with SD-1 seismographs is shown in Fig. 1. At the present time, 15 SD-1 seismographs operate continuously (see Table 1)

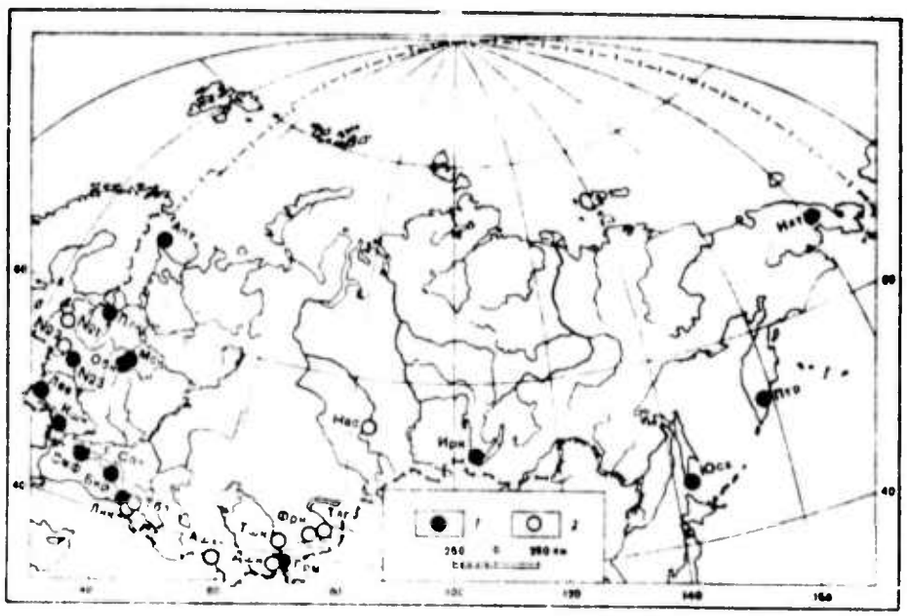

Fig. 1. Location of seismic stations equipped with SD-1 seismographs.

1 - operating; 2 - nonoperating or irregularly operating.

Table 1

Seismic seismographs stations equipped with SD-1
(through the first half of 1972)

No.	Station	Beginning of operation	Magnification N-S	E-W	Z	Note
1.	Apatity	Aug. 1970	-	-	970	
2.	Bakuriani	Dec. 1971	-	-	560	From June 1972 V_z = 1400.
3.	Garm	Jan. 1968	100	100	-	In 1968-70 magnification was 800.
4.	Irkutsk	March 1971	200	200	200	
5.	Iul'tin	June 1970	1000	980	980	
6.	Kishinev	Jan. 1970	-	-	1080	In Oct. 1972 horizontal components with magnification 750 were installed.
7.	L'vov	July 1969	-	-	900	In July 1972 horizontal components installed
8.	No. 3	Jan. 1971	770	770	750	Jan. 1971 - Jan. 1972 only horizontal components.
9.	Moskva	Jan. 1968	-	-	1070	
10.	Obninsk SD-2(1) Press-Ewing	Jan. 1967 July 1966	830 800	830 800	830 1900	
11.	Petropavlovsk	May 1969	1100	1100	1050	From July 1972 magnifications are 860, 960, 960.
12.	Pulkovo	Feb. 1970	-	-	100	
13.	Simferopol'	Nov. 1970	830	830	980	From Nov. 1969 only vertical component.
14.	Sochi	Aug. 1971	-	-	(1500)	
15.	Yuzhno-Sakhalinsk	Feb. 1967	1000	1000	1000	Press-Ewing seismograph

The SD-1 seismograph, consisting of SKD seismometer (T_s = 25 sec) and SPG galvanometer (T_g = 80-100 sec), is characterized by a passband of 15-60 sec at the 0.9 level and maximum magnification of 1500. Its threshold sensitivity at V_m = 700-1000 was determined to be $m_{PV_{min}}^{SD-1}$ = 6 for epicentral distances Δ = 20-100°. Its dynamic range is not sufficient for recording PV and m_{PV} = 7 (Δ = 20-40°). At least three sources of long-period noise were identified during operation of SD-1 seismographs at different stations: wind, industrial and civilian activity, and fluctuations in atmospheric pressure and temperature.

The records of the same earthquakes made by SD-1 seismographs installed at different stations are characterized by:

1. High stability of waveform of body waves for stations with similar epicentral distance and azimuth (Fig. 2);

2. Stable pattern of dispersion of R waves within a period range from 60 to 15-20 sec but with amplitude modulation (Fig. 3). Fig. 4 illustrates the difference in amplitude of L surface waves from the earthquake of 5 May 1972 originating in the Solomon Islands recorded at different stations, which is suggested to be due to high directivity of seismic radiation.

3. Distinguishable R_2 surface waves from earthquakes with M = 6.5 - 6.75 (Fig. 5).

4. High stability of m_{PV} evaluated from these records (Table 2).

The fully operational SD-1 seismographs provide for study of the earth structure along the following profiles and triangles:

1. a. Apatity-Pulkovo-No. 3-Kishinev (Aleutions, Balkans);
   b. Apatity-Pulkovo-Obninsk-Simferopol' (Alaska, Turkey, Red Sea, East Africa);
   c. Apatity-Obninsk-Sochi (Vancouver, Tuamotu Archipelago, Red Sea, East Turkey, Madagascar);
   d. Kishinev-Simferopol'-Sochi-Bakuriani (Azores, Central America, Iran, West Indonesia, New Zealand).

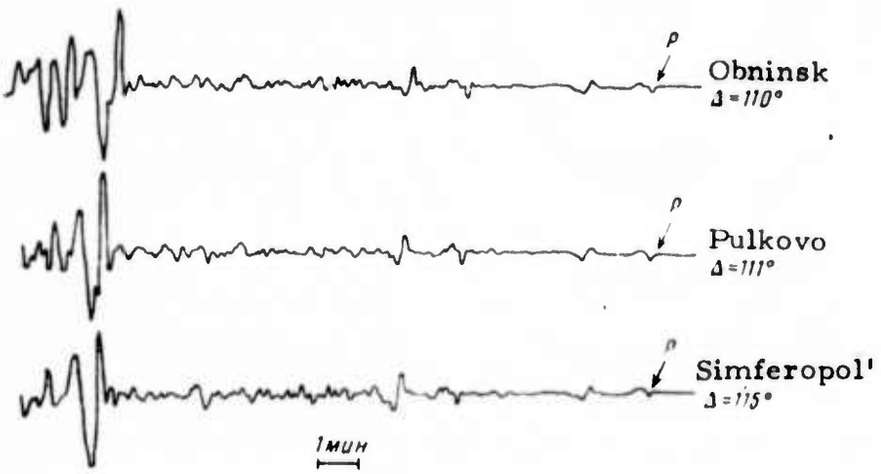

Fig. 2. Records of the earthquake of 28 April 1972 in the Solomon Islands region made by vertical SD-1 seismographs. Note identical waveform of body waves and prominent diffracted P wave.

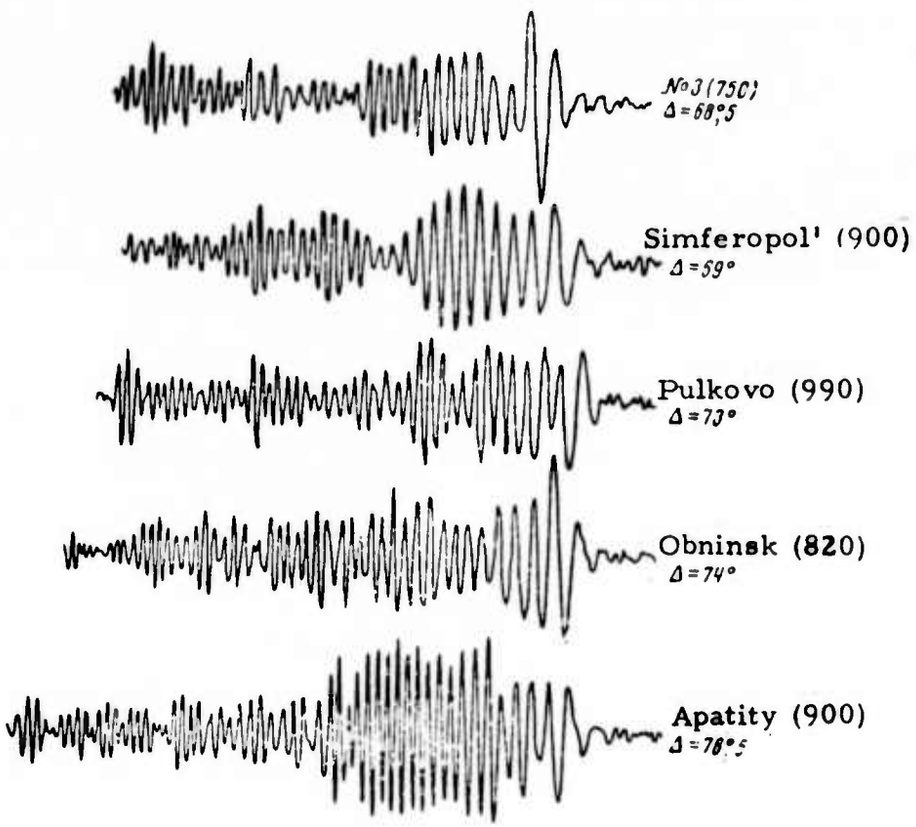

Fig. 3. Records of R surface waves from the earthquake of 11 April 1972 in the North Atlantic ridge, made by SD-1 seismographs.

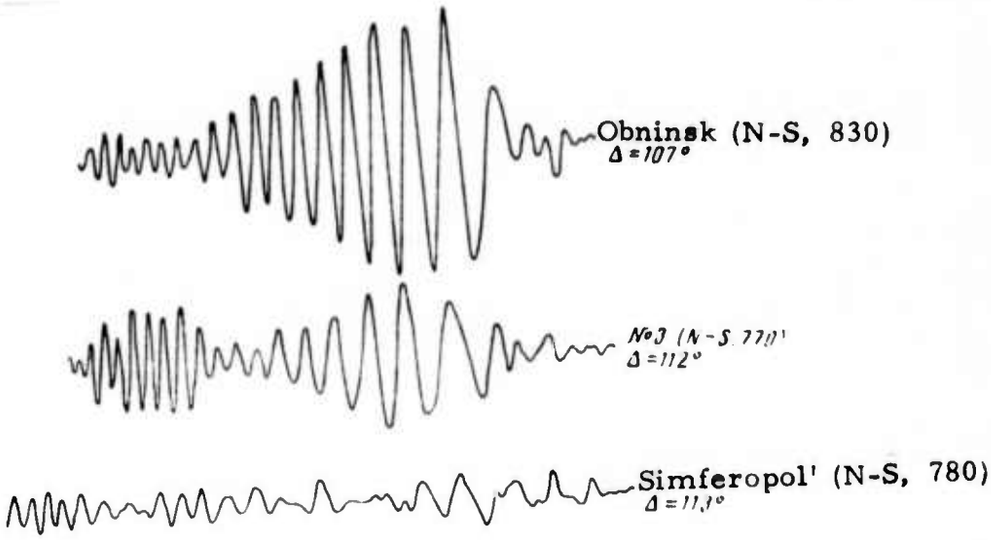

Fig. 4. Records of L surface waves from the earthquake of 5 May 1972 in the Solomon Islands region, made by SD-1 seismographs.

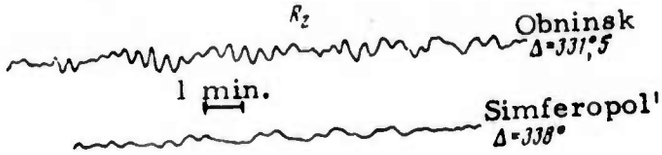

Fig. 5. Records of R_2 surface waves from the earthquakes of 10 April 1972 in Iran, made by SD-1 seismographs.

Table 2

Earthquake magnitudes determined from SD-1 records

Earthquake	Station	Δ°	m_{PV}	m_{PH}	T_{PV}, sec	T_{PH}, sec	Note
10 April 1972, Iran	Garm	18	-	6.6	-	14	From data
(φ = 28.5°N,	Sochi	19	6.3	-	22	-	of 5 stations
λ = 52.8°E,	Simferopol'	22	6.6	6.6	17	15	$\bar{T}_{SH}$ = 26±4 sec
m_{PV}^{SK} = 6.8,	Kishinev	26	6.5	-	18		
$\bar{M}$ = 6.8)	Obninsk	29	6.7	6.8	16	16	$\bar{T}_{SH}/\bar{T}_{PV}$ = 1.63
	No. 3	31	6.6	-	16	-	
	Pulkovo	35	6.6	-	16	-	
	Apatity	40	6.6	-	16	-	
	Irkutsk	45	6.7	-	16	-	
	Yuzhno-Sakhalinsk	69	6.6	6.8	12	-	
	Iul'tin	76	6.6	6.5	14	10	
	Petropavlovsk	76	6.6	-	14	15	
			6.6±0.05	6.7±0.1	16±2	14±2	
11 April 1972,	Kishinev	67	6.4	-	14	-	
North Atlantic	No. 3	69	6.6	-	14	-	
ridge (φ = 1.2°N,	Simferopol'	70	6.5	-	14	-	
λ = 28.4°W,	Pulkovo	74	6.5	-	13	-	
m_{PV}^{SK} = 6.8,	Sochi	74.	6.6	-	12	-	
$\bar{M}$ = 6.6)	Obninsk	75	6.6	-	12	-	
	Apatity	78	6.4	-	13	-	
			6.5±0.05		13±1		

2. a. No. 3-Obninsk-Pulkovo (600±50);
   b. L'vov-No. 3-Kishinev (600±150);
   c. Kishinev-No. 3-Obninsk (800±200);
   d. Simferopol'-Obninsk-Kishinev (850±350);
   e. Simferopol'-Obninsk-L'vov (1000±100).

Feofilaktov, V. D., and V. A. Masloboyev. Comparison of dynamic characteristics of standard high-sensitivity seismographs used in the USA and USSR. Fizika Zemli, no. 1, 1975, 95-100.

A comparative analysis was made of systematic distortion of the shape of the records of P waves introduced by narrow-band SKM-III and Benioff seismographs. The effect of self-inductance on the motion of the narrow-band Benioff seismograph was considered and an analytical expression for its response to simple harmonic earth motion was developed by the method of electromechanical analogy.

The analog circuit for Benioff seismograph used in the analysis is shown in Fig. 1. An analysis of the formula shows that for $T \to 0$ $U \to T^2/T_L$, and for $T \to \infty$ $U \to 1/sT^3$. The response curve of the Benioff seismograph calculated by the derived formula is shown in Fig. 2.

The comparative analysis was performed in terms of $A^* = \lg A/T$ corresponding to maximum pulses, using records of 196 earthquakes (Δ = 11-103°; h from normal to 530 km; M_{PV} = 4.47-7.3) made at the Obninsk station in 1970. The apparent periods ranged from 0.4-2.0 sec.

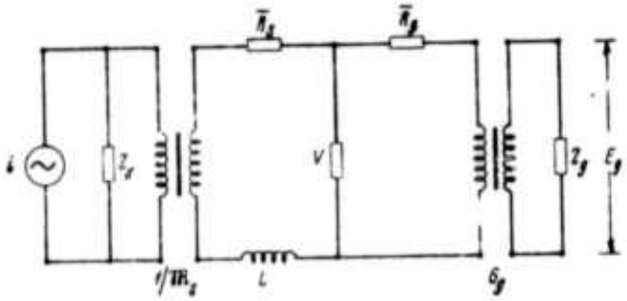

Fig. 1. Electric analog for Benioff seismograph.

i- analog to inertial force $j\omega m_s \dot{X}$;
E_g - angular velocity $\dot{\varphi}$ of the galvanometer frame;
$\bar{R}_s = R_s + R_1$, $\bar{R}_g = R_g + R_2$;

L- self-inductance of the seismometer coil;

$1/m_s$ - electromagnetic converter with constant m_s;

Gg- magnetoelectric converter with constant Gg;

$Z_s = 1/(j\omega m_s + 2\varepsilon_{s0} n_s^2 m_s/j\omega)$,

$Z_g = 1/(j\omega K_g + 2\varepsilon_{g0} K_g n_g^2 K_g/j\omega)$,

where ϵ_{s0} (ϵ_{g0}), n_s (n_g), and k_g are air damping coefficient, angular frequency, and moment of inertia, respectively.

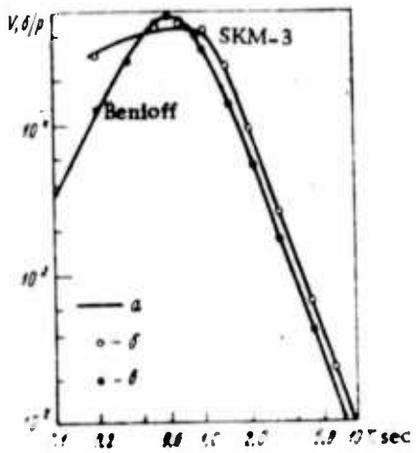

Fig. 2. Response curves of SKM-III and Benioff seismographs.

a- calculated, b and c- experimental.

The variation of $\Delta A^* = A^*_{SKM} - A^*_B$ with apparent periods T_{SKM} is shown in Fig. 3. The results of statistical analysis of ΔA^* and $\Delta T = T_{SKM} - T_B$ for six separate period intervals are given in Tables 1 and 2. The variations of the average values of ΔA^* and ΔT with the average values of T_{SKM} calculated for the six period intervals are shown in Fig. 4.

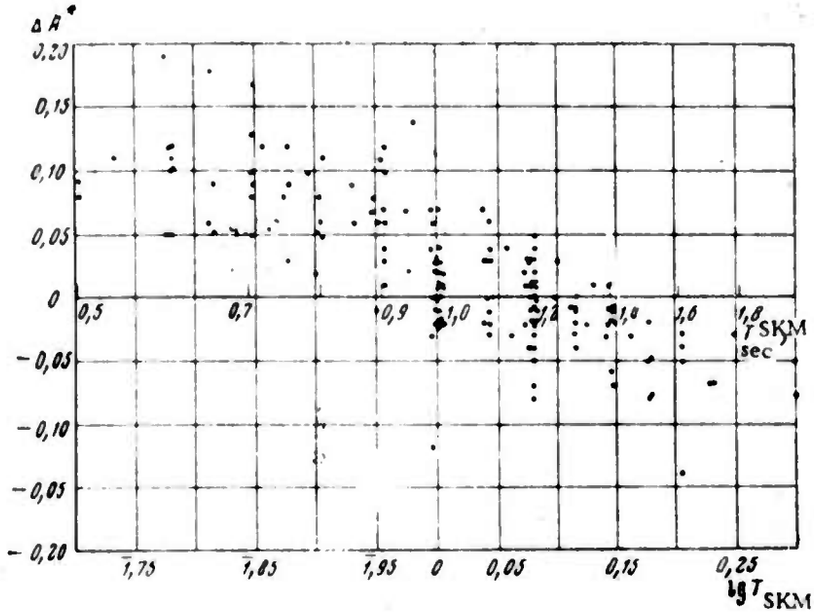

Fig. 3.

It is concluded that discrepancies between lg A/T and T determined from the records of SKM-III and Benioff seismographs are highest in the period range 0.6-1.0 sec. Namely, values of lg A/T determined from the records of the Benioff seismograph are lower by 0.1 than the corresponding values determined from the records of SKM-III seismograph.

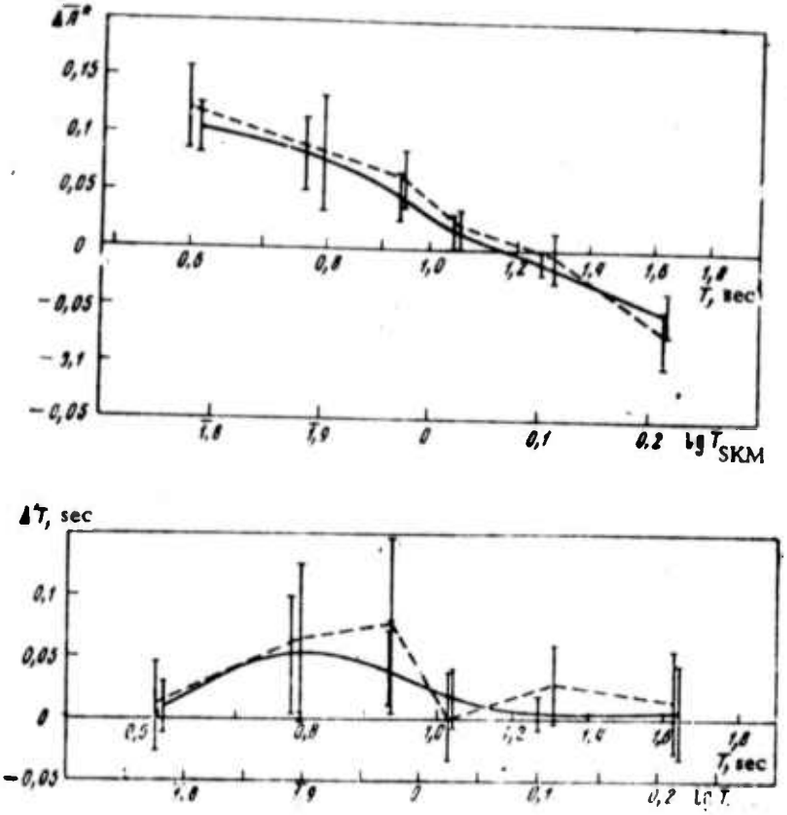

Fig. 4.

Table 1

	I	II	III	IV	V	VI
n	27	16	31	37	61	17
$\overline{\Delta A}°$	+0,104	+0,082	+0,045	+0,015	−0,011	−0,056
S^2	0,00168	0,00196	0,00175	0,00133	0,00068	0,00082
S	0,041	0,045	0,042	0,036	0,026	0,029
$\overline{S}$	0,0079	0,0115	0,0075	0,0059	0,0033	0,0070
d	0,022	0,034	0,021	0,016	0,009	0,020
$\overline{\lg T}_{SKM}$	1,789	1,885	1,974	0,022	0,101	0,218

Table 2

	I	II	III	IV	V	VI
n	12	11	25	21	24	6
$\overline{\Delta T}$	+0,008	+0,050	+0,036	+0,014	+0,003	+0,004
S^2	0,00053	0,00256	0,00380	0,00156	0,00051	0,00054
S	0,0230	0,0505	0,0615	0,0396	0,0226	0,0234
$\overline{S}$	0,0066	0,0152	0,0123	0,0084	0,0046	0,0096
d	0,0206	0,0481	0,0344	0,0238	0,0129	0,0385
$\overline{\lg T}_{SKM}$	1,782	1,891	1,976	0,029	0,101	0,217

Nersesov, I. L., Ye. I. Gal'perin, L. M. Vorovskiy, and R. M. Gal'perina. Alma-Ata high-sensitivity radiotelemetric seismograph test site. IN: Fizika Zemli, no. 7, 1974, 72-77.

A brief description is given of the set up and instrumentation of the seismograph stations of the Alma-Ata test site, as well as the initial results of its operation.

The location and set up of the seimograph stations are illustrated in Fig. 1 and Table 1. The network consists of underground stations set up in deep boreholes (I, V, and VII in Fig. 1) and surface stations (II, III, IV, and VI). The underground stations are equipped with SBU-V seismometers with natural periods of 1.0 sec and preamplifiers with negative feed-back having flat temperature curves up to 45° C. The surface stations are equipped with SM-2M seismometers with natural frequencies of 1 Hz and the same type of preamplifliers. The signals are transmitted to the central station at Novo-Alekseyevka (VII in Fig. 1). The power of the transmitters (with power amplifier units) is 25 w; without, it is 2.5 w. The transmission of information via RRS-1M radio relay stations is based on double conversion FM-FM. Signals are recorded on the same strip chart by an RVZ-T visual recording system. They are recorded on magnetic tape as well as coded using an Udar-1M analog-to-digital converter.

The reading accuracy for time differences in $\pm$ 0.2 sec in the case of visual recording and $\pm$ 0.03-0.05 for magnetic recording. Epicentral coordinates are determined using computer-generated nomograms for given focal depths (see Fig. 2).

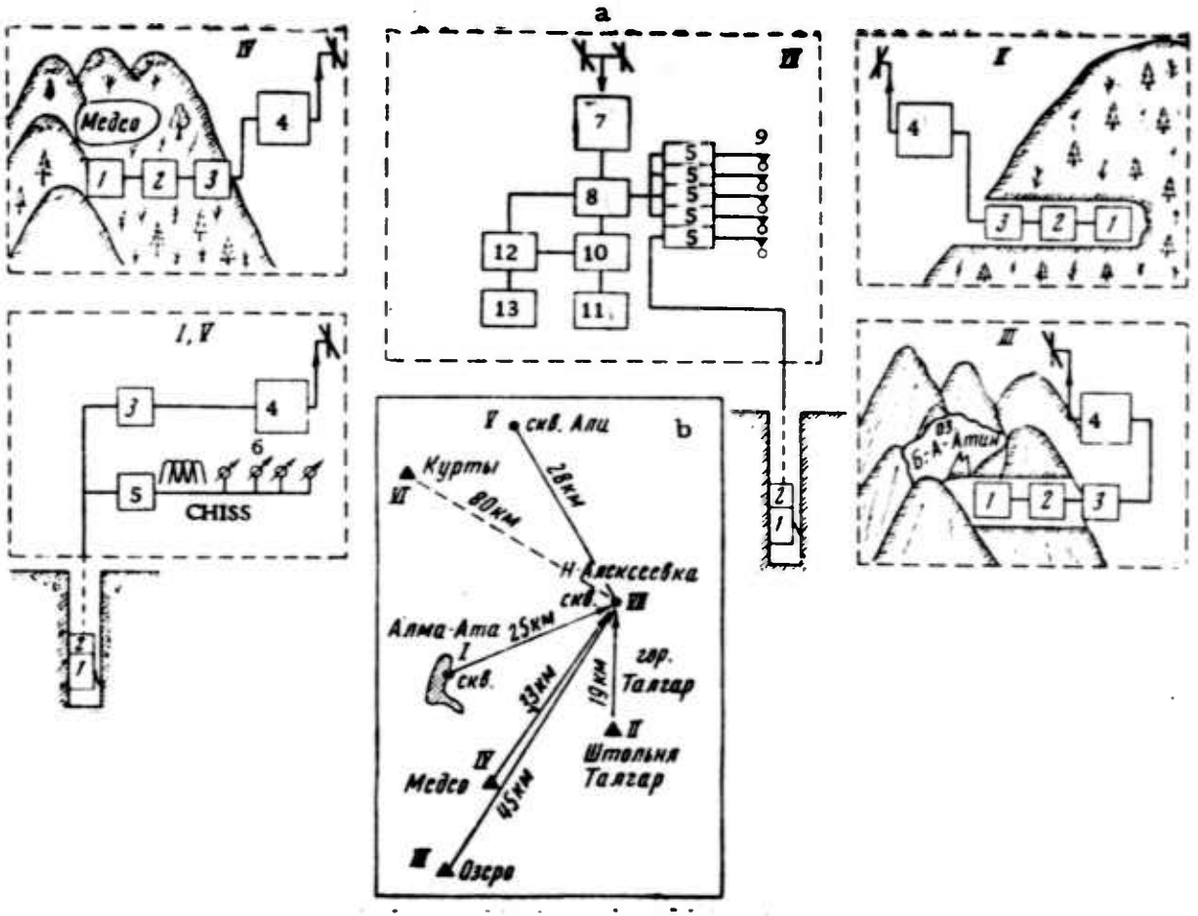

Fig. 1. Arrangement of the Alma-Ata Radio-Telemetering Seismograph Test Site.

a- Block diagram of transmitter stations; I- Borehole-10; II- Shtol'nya tunnel; III- Ozero; IV- Medeo; V- Borehole Ali; VI- Kurty; VII- central recording station in Borehole-1 at Novo-Alekseyevka; 1- seismometer; 2- preamp; 3- modulators; 4- transmitter; 5- power amplifier; 6- galvanometers; 7- radio receiving station; 8- demodulator; 9- pen recorder; 10- coding unit; 11- mag tape recorder; 12- recording delay unit; 13- oscillograph; CHISS- frequency-selective seismic system.

Table 1

Station	Magnification	Depth	Note
I (Alma-Ata)	$5\text{-}6 \cdot 10^5$ - $1 \cdot 10^6$	2000 m	In sedimentary rock. Crystalline basement top at 4200 m.
II (Talgar)	$3\text{-}4 \cdot 10^5$	120 m	In crystalline rocks. Crystalline basement exposed.
III (Ozero)	$1 \cdot 10^6$	-	
V (Ali)	$3\text{-}4 \cdot 10^5$ - $8\text{-}9 \cdot 10^5$	800 m	In sedimentary rocks. Crystalline basement top at 860 m.
VII (Novo-Alekseyevka)	-	2985	In crystalline rocks. Crystalline basement top at 2960 m.

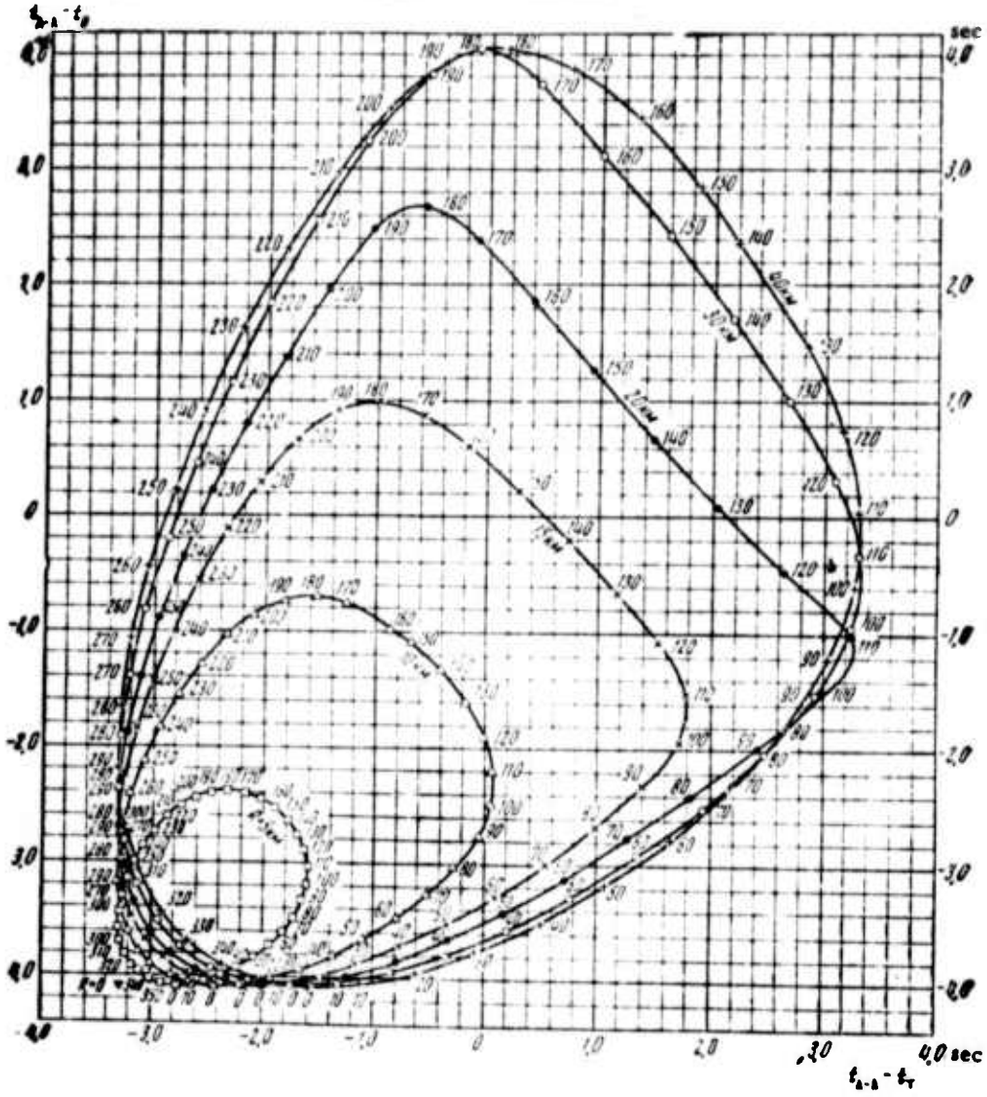

Fig. 2. Sample Nomograms Used for Determining Epicentral Coordinates.

t_{A-A} - first-arrival time at Alma-Ata station;

t_T - at Talgar;

t_0 - at Ozero;

R - epicentral distance from the Alma-Ata station.

Rykov, A. V. Calculation of the main parameters of a magnetoelectric seismograph. IN: Fizika Zemli, no. 7, 1974, 78-83.

A method was described for calculation of the parameters of a seismometer-galvanometer system based on the feedback ratio concept. The calculated parametes were used for determining resistance in seismograph circuits.

In the calculation of the maximum magnification V_{max} of a seismograph for the case of a given response curve, the curve is specified graphically in Fig. 1. Accordingly, the coefficients in the response equation

$$U = \eta(\gamma T^{-2} + \alpha + \beta T^2 + \gamma T^4 + \delta T^6)^{-1/2}, \quad (1)$$

are found from the system of equations

$$U(T_1) = 0.7;\ U(T_2) = 1.0;\ U(T_3) = 1.0;\ U(T_4) = 0.7;\ U(T_5) = 0.15.$$

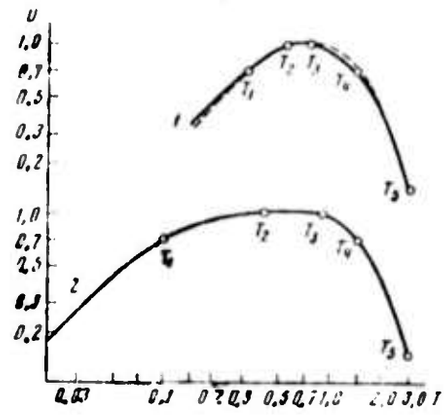

Fig. 1. Pre-set response curves for an SKM-3 seismograph of the standard type III (1) and IV (2).

The maximum magnification is then calculated using formula

$$V_{max} = \frac{2A}{\eta l}\sqrt{\frac{K_0}{K_g} k_{max}},$$ where A is the optical arm of the galvanometer,

l is the reduced pendulum length of the seismometer, k_s and k_g are inertia moments, η is the bandwidth factor, and k_{max} is feedback ratio.

In calculating seismograph parameters in the case of a given magnification level, the desired magnification is expressed in terms of the magnification factor $F = \xi F_{max}$, where $\xi = V/V_{max}$ is the gain reduction factor and $F_{max} = k/T_g^2$.

The table below gives the parameters of an SKM-3 seismograph, standard type IV, for various magnifications and the parameters of an SKD seismograph for the maximum and standard magnification.

Table 1

$V \cdot 10^4$	h	T_s	D_s	T_g	D_g
			SKM-3		
7,65	0,382	2,268	0,683	0,314	1,561
6,0	0,324	1,928	0,711	0,369	1,812
5,0	0,283	1,721	0,701	0,414	2,014
4,5	0,252	1,640	0,686	0,434	2,108
4,0	0,215	1,579	0,667	0,451	2,188
3,5	0,174	1,534	0,648	0,464	2,252
3,0	0,134	1,501	0,631	0,474	2,302
2,5	0,096	1,477	0,617	0,482	2,341
2,0	0,069	1,459	0,605	0,488	2,372
1,5	0,036	1,446	0,595	0,493	2,394
			SKD		
1,0	0,228	28,3	0,468	1,038	6,884
0,1	0,0031	25,0	0,500	1,200	8,000

Tokmakov, V. A. OSP seismometer and its experimental exploitation. Trudy Instituta fiziki Zemli AN SSSR, no. 16, 1974, 147-152.

The OSP seismometer, developed jointly in 1968-69 by the Institute of the Physics of the Earth (Soviet Academy of Sciences) and the Special Design Office of the Institute of Geophysics and Engineering Seismology (Armenian Academy of Sciences) is described. A general view of the seismometer is shown in Fig. 1 and its cross section, in Fig. 2. The OSP seismograph circuits are shown in Fig. 3.

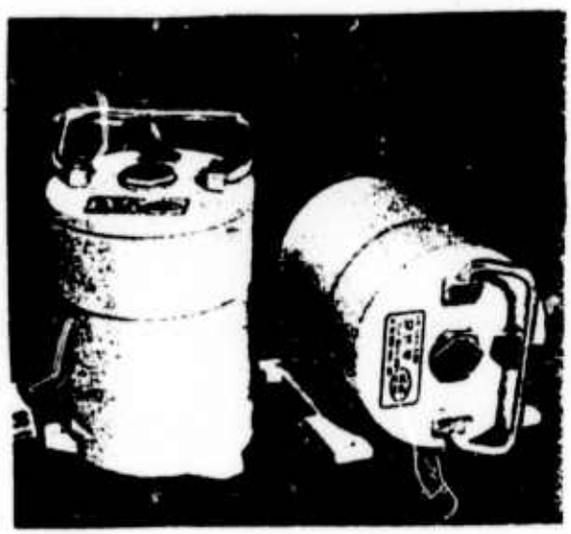

Fig. 1. General View of the Vertical OSPV and Horizontal OSPG Seismometers.

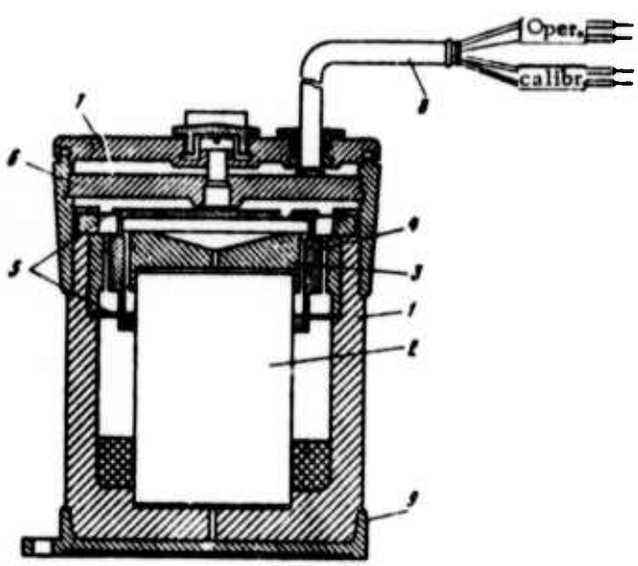

Fig. 2. Cross-Section of the OSP Seismometer.

1- magnetic-circuit casing; 2- permanent magnet; 3- pole piece; 4- induction coil; 5- springs; 6- interior cover; 7- main cover; 8- 4-conductor cable; 9- base.

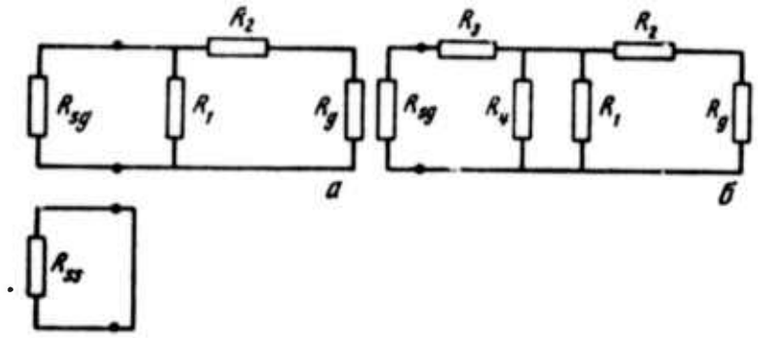

Fig. 3. Electric Circuits of the OSP Seismograph.

R_{sg} - operating coil; R_{ss} - calibrating coil; Rg - galvanometer; R_1-R_4 - resistances.

The specifications of the OSP seismometer are as follows:

1.	Mass of suspended system M_s, kg	$4 \cdot 10^{-2}$
2.	Natural frequency f_s, H_z	5
3.	Resistance of operating coil R_{sg}, Ohm	11
4.	Sensitivity of operating coil m_{sg}, V/m/sec	15
5.	Sensitivity of calibrating coil M_{ss}, V/m/sec	5.5
6.	Damping D_s, in fractions of critical damping	7
7.	Limit velocity, m/sec	1.25
8.	Water-tightness, in meters of water column	1.0
9.	Weight, kg	4.6

High damping is achieved using aluminium wire for the induction coil.

The OSP seismograph is used mainly for recording the velocity and acceleration of ground motion. For the former, the GB-III (5 H_z) and M002 (25 H_z, D_g = 15) galvanometers are used; for the latter, GB-IV (120 H_z) and M002 (120, 400 H_z) galvanometers and the N-735 loop-type [recorder] are used.

Beskorovaynyy, V. L., V. P. Marukhnenko, G. S. Sokolov, and A. M. Yampol'skiy, Gain control for selection signals for a digital seismic system. Othrytiya, izobreteniya, promyshlennyye obraztsy, tovarnyye znaki, no. 18, 1974, 129. (Author Certificate 428328).

A patent has been issued for the above, containing a cascade amplifier, a logic circuit for amplification selection for each selection signal, and switches for commutation of the outputs from the amplifier stages. To reduce the equipment, a converter of selection signal polarity, a coincidence circuit, and a trigger with voltage output are series connected between the outputs of the amplifying stages and the logic circuit inputs.

Beskorovaynyy, V. L., V. P. Marukhnenko, G. S. Sokolov, and A. M. Yampol'skiy. Digital multichannel seismic system. Otkrytiya, izobreteniya, promyshlennyye obraztsy, tovarnyye znaki, no. 18, 1974, 129. (Author Certificate 428329).

A patent has been issued for the above, containing preamps connected through a channel commutator (having a control circuit) to the main amplifier which has digital gain control. In order to increase the dynamic range, each channel in the system has a series connected delay line and an additional amplifier with digital gain control connected between the preamp output and the channel commutator input. The additional amplifier is connected to the output of an additional control circuit whose inputs are connected to at least two sections of the delay line and the channel commutator control circuit.

Slutskovskiy, A. I., S. V. Nikiforov, A. I. Vasik, and V. I. Korinnyy. Method of recording ground motion. Otkrytiya, izobreteniya, promyshlennyye obraztsy, tovarnyye znaki, no. 18, 1974, 129. (Author Certificate 428330)

A patent has been issued for the above method which is based on the exposure of photosensitive material to a light beam from a controllable source. To improve visual correlation, the signal being recorded is split into two channels. In the first channel, the signal is converted into a voltage corresponding to one type of recording, while the signal in the second channel modulates the recording brightness. In this method, the signal shape is changed in the second channel, for example, it is optimized, high-frequency modulated, or clipped.

2. Computer Seismology

Gerver, M. L., V. I. Keylis-Borok, Yu. A. Kolesnikov, A. L. Levshin, V. M. Markushevich, B. M. Naymark, and V. F. Pisarenko. Problems of global computational geophysics. Fizika Zemli, no. 10, 1974, 33-45.

A review is given of the work in global computational geophysics performed by researchers of the Institute of Physics of the Earth, the Institute of Applied Mathematics and Chemical Physics of the USSR Academy of Sciences, and the Moscow and Leningrad State Universities since 1960. The problems considered included automation of primary analysis, the inverse seismological problem, mathematical modeling, recognition algorithms, and evaluation of seismic hazard.

The results achieved are illustrated in Figs. 1-7.

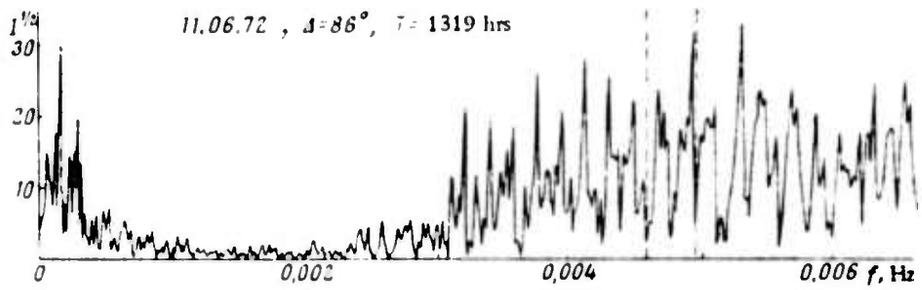

Fig. 1. Spectrum of a strong earthquake recorded by the SDS-300 seismograph at the Obninsk station.

Length of record - 10-16 hours;
number of readings - 10-16 thousand.
Sharp peaks are identified with natural frequencies of spheroidal oscillations of the Earth.

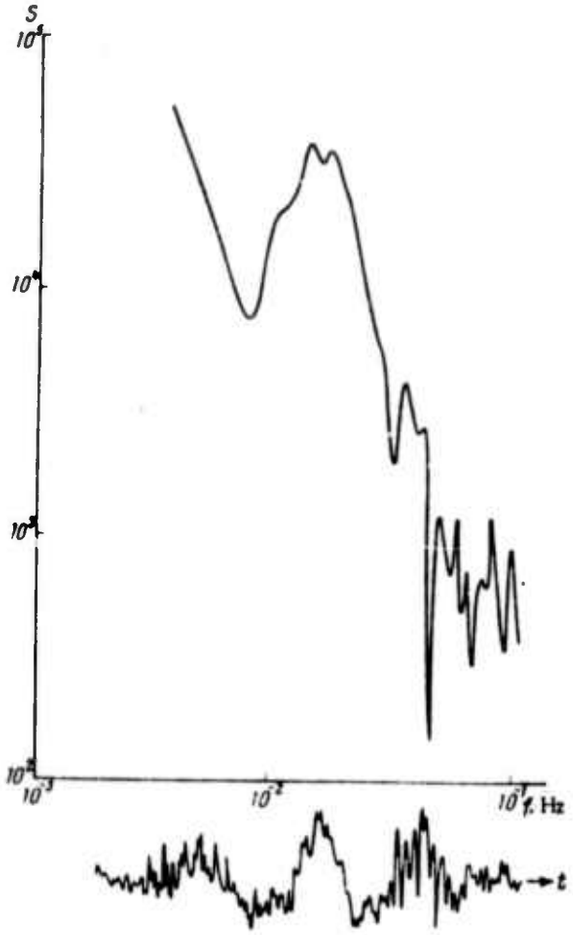

Fig. 2. Seismogram and spectrum of S waves from the destructive Kamchatka earthquake of 24 Nov. 1971 recorded by digital equipment at the Naryn station.
High energy is concentrated in the 50-100 sec range.

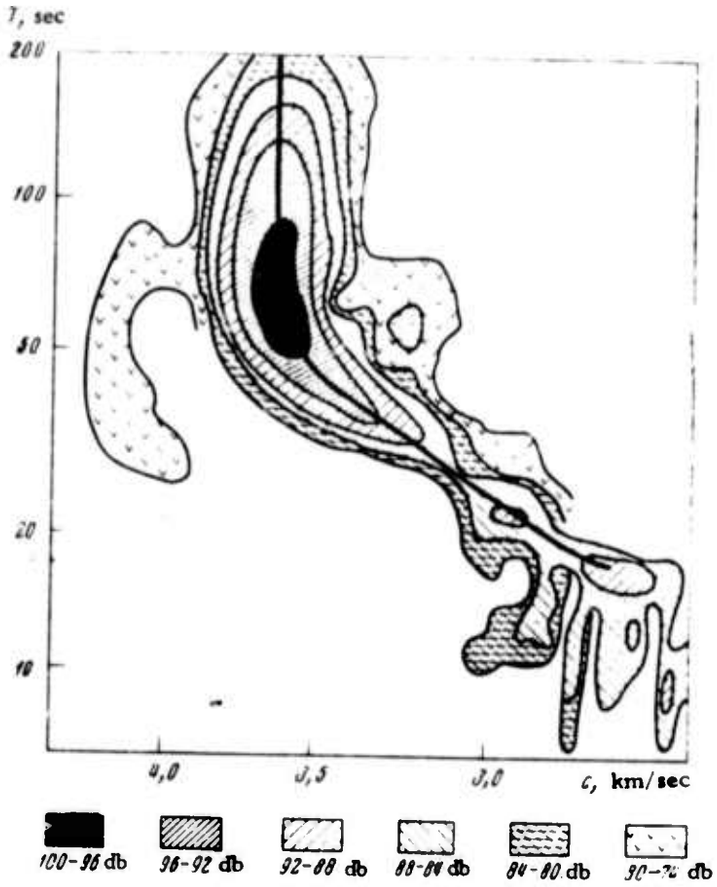

Fig. 3. Surface waves from the destructive Kamchatka earthquake of 24 Nov. 1971 studied using the frequency-time method.
Group velocity of Rayleigh waves is reliably determined.

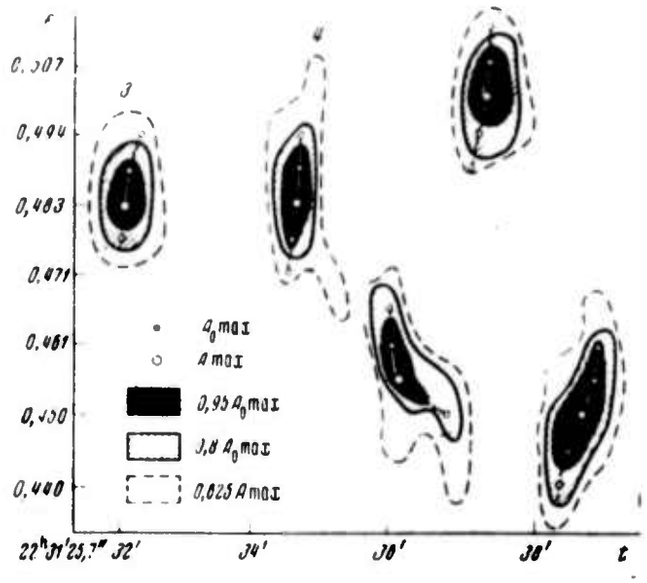

Fig. 4. Use of the frequency-time analysis in study of hydromagnetic waves (3 December 1965, Kerguelen). A hydromagnetic wave is split into two waves shifted in phase.

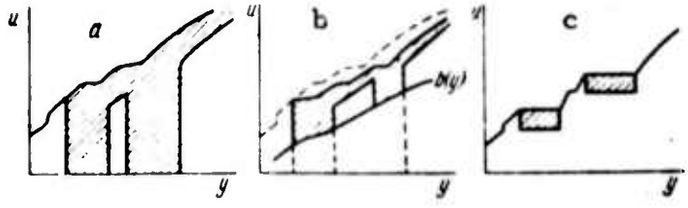

Fig. 5. Determination of velocity distribution from time-distance curves for refracted waves from a surface source

a- in the case of two waveguides; b- u(y) limited by b(y); c- additional time-distance curves for refracted waves from two deep-seated sources between and below waveguides.

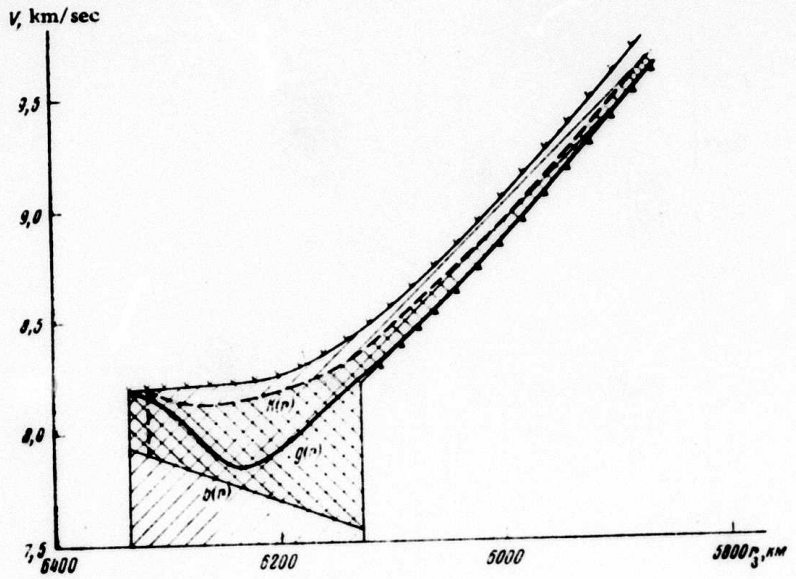

Fig. 6. Gutenberg curve g(r) and one of "concurrent" solutions k(r).

Cross hatching- velocity distribution in the waveguide $v(r) \geq b(r)$.

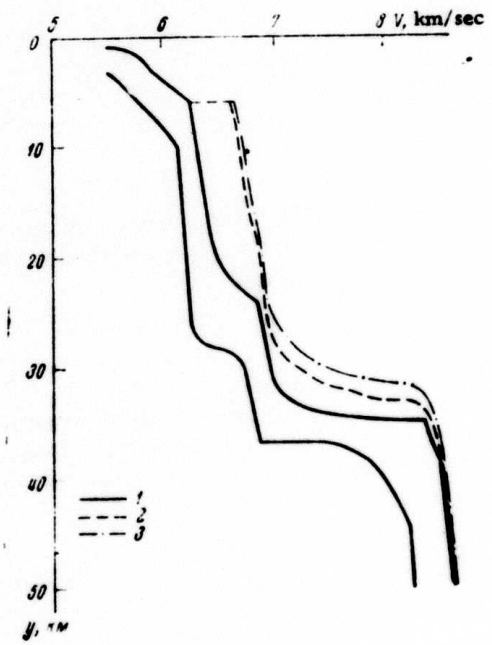

Fig. 7. Velocity distributions inferred from data from deep seismic sounding in the Central Turkmen to 1962-64.

1- no waveguide is assumed; 2- a waveguide with velocity to 6 km/sec; 3- a waveguide with velocity to 5.5 km/sec.

Lander, A. V., A. L. Levshin, V. F. Pisarenko
G. A. Pogrebinskiy, and O. Ye. Starovoyt.
Extraction of natural oscillations of the Earth from records of the Obninsk observatory. IN:
Vychislitel'naya seysmologiya, no. 7, Moskva,
Nauka, 1974, 315-331.

The data on earthquakes used for calculations of natural oscillations of the Earth are given in Table 1. The frequency response of the long-period vertical seismograph used for recording is shown in Fig. 1.

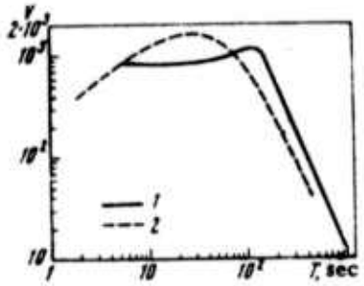

Fig. 1. Magnification curves of vertical seismograph SDS-300 (1) and Press-Ewing (2).

The calculated values of periods of identified fundamental ${}_0S_n$ ($12 \leq n \leq 50$) and overtone ${}_kS_n$ ($k>0$) oscillations of the Earth are given in Tables 2 and 3, respectively; values of quality factor Q are in Fig. 2. Dispersion curves determined from data on travelling waves are shown in Fig. 3.

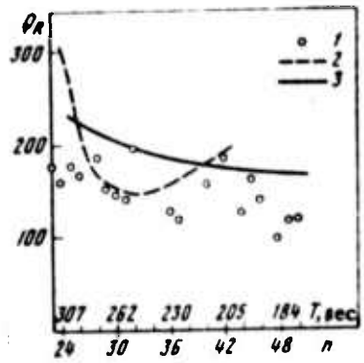

Fig. 2. Q_R for fundamental spheroidal oscillations from standing (1) and travelling (2) waves, and according to Anderson, 1967 (3).

Table 1

No.	Data on earthquakes								Data on records			
	Date and time GMT	Region	φ, °	λ, °	H, km	Δ, °	M	Seismograph	t_H, GMT	$\tau = t_k - t_{Hgh}$	t, sec	N
1	11 June 1970 $16^h46^m38^s$	South of Macquarie Is.	59.1 S	157.8 W	33	148.7 16532 km	7.2	SDS 300 Z	$17^h30^m00^s$	9.0	3.25	10045
2	31 July 1970 $17^h08^m06^s$	Columbia	1.5 S	72.6 W	650	102.1 11355 km	7.1	SDS 300 Z	$17^h52^m00^s$	12.1	3.37	12962
3	11 June 1972 $16^h41^m02^s$	North from the Sulawesi Is.	3.9 N	124.5 E	330	85.6 9520	7.4	SDS 300 Z	$17^h41^m00^s$	13.3	3.25	14762
4	2 December 1972 $00^h19^m48^s$	Mindanao Is.	6.4 N	126.9 E	60	85.0 9450	7.1	Press-Ewing Z	$01^h44^m11^s$	9.3	3.16	10647

Periods of spheroidal oscillations ${}_0S_n$

n	Earthquakes						Average from 1, 2, 3, and 4	Theoretical values (Dziewonski and Gilbert, 1972)
	1	2	2a	2b	3	4		
12	-	502.22	-	503.62	-	-	502.22 (1)	502.90
13	471.97?	474.27?	-	472.91	-	-	473.15 (2)	473.70
14	448.45?	448.67	-	448.09	-	-	448.56 (2)	448.54
15	-	426.13	-	-	-	-	426.13 (1)	426.55
16	-	406.52	-	407.68	407.08?	-	406.80 (2)	407.15
17	390.06	390.13	-	388.97	390.21?	390.41	390.20 (4)	389.88
18	374.24	-	-	374.87	373.44?	375.11	374.26 (3)	374.39
19	360.30	360.16	359.0	359.97	360.70?	-	360.39 (3)	360.41
20	346.97	347.45	347.0	347.73	347.70?	-	347.37 (3)	347.72
21	335/34?	336.22	334.5	335.58	335.63?	336.19	335.84 (4)	336.15
22	-	325.71	324.0	324.94	324.64	-	325.18 (2)	325.49
23	315.91	314.95	314.5	314.31	315.32	-	315.39 (3)	315.49
24	306.88	306.59	306.0	306.78	306.39	306.15?	306.50 (4)	306.36
25	298.03	297.04?	297.5	297.45	297.50	297.89	297.61 (4)	297.79
26	290.28	289.66	289.5	290.16	289.49	290.15?	290.10 (4)	289.82
27	282.53	282.92	282.0	282.67	282.39	281.47	282.33 (4)	282.33
28	-	275.23	275.0	275.80	274.51	275.44	275.39 (3)	275.27
29	268.41	269.46	268.5	268.56	268.39	268.08	268.64 (4)	268.59
30	262.05	261.97	262.0	262.02	261.85?	262.59	262.12 (4)	262.25
31	256.13	256.41	256.0	255.69	255.96	255.70	256.05 (4)	256.22
32	250.68	249.99	250.0	249.96	250.65	250.55	250.47 (4)	250.48
33	244.62	245.29	245.0	245.13	244.70	244.49	244.77 (4)	245.00
34	239.61?	239.74	239.5	239.23	239.64?	240.02	239.75 (4)	239.76
35	234.76	234.67	235.0	234.48	234.36	234.47?	234.56 (4)	234.74
36	230.02	230.29?	230.0	-	-	229.97?	230.09 (3)	229.98
37	225.43	225.27	225.5	225.18	224.72	224.78?	225.55 (4)	225.30
38	220.99	221.05	221.0	220.47	220.73?	221.03	220.45 (4)	220.86
39	216.27?	216.45	217.0	217.28	216.17?	-	216.30 (3)	216.59
40	212.50?	212.51	212.5	211.80	212.53?	212.12	212.42 (4)	212.48
41	208.45	-	208.5	208.00	208.19?	208.36?	208.33 (3)	208.51
42	204.73	204.54	204.5	204.87	204.69	204.54	204.62 (4)	204.68
43	201.16	-	201.0	200.91	-	-	201.16 (1)	200.99
44	197.44?	197.01	-	196.73	197.79	-	197.41 (3)	197.43
45	194.10?	194.13	-	194.17	-	194.23	194.15 (3)	193.98
46	-	190.45?	-	190.40	190.63	190.41	190.50 (3)	190.64
47	-	187.48	-	187.82	-	187.54	187.51 (2)	187.42
48	184.44	183.89?	-	184.34	183.96?	184.54	184.21 (4)	184.30
49	181.60	181.66?	-	181.60	181.44	181.64	181.58 (4)	181.27
50	178.63	178.98?	-	177.84	178.01	178.17	178.45 (4)	178.34

Note: 2a- according to Nawroozi, 1972
2b- determined from R_2, R_4.

Table 3

Periods of overtone spheroidal oscillations

Overtone	Earthquakes					Theoretical values (Dziewonski and Gilbert, 1972)
	1	2	2a	3	4	
1^S16	-	-	-	300.21?	-	299.46
1^S17	-	287.06?	285.68	285.32	287.21?	286.15
1^S19	-	-	-	263.10	-	263.59
1^S20	253.31	-	-	-	-	-
1^S22	-	238.16	-	237.48	-	-
1^S23	-	228.51	-	227.94?	-	-
1^S25	-	-	-	213.83	-	-
2^S10 or 3^S5	-	416.44?	415.76	416.53?	-	415.77, 414.94
2^S12	-	366.54	366.26	364.46?	-	365.05
2^S13	-	-	-	343.99	-	-
2^S20	-	-	-	-	232.55?	232.50
3^S3	-	-	489.60	488.18?	-	488.51
3^S7	-	371.76	370.91	-	-	372.71
3^S11	311.21	311.85?	310.66	-	-	310.62
4^S6	-	331.62	-	332.06	-	332.58
4^S7	302.65	303.27	302.22	-	-	332.58
4^S10 or 2^S13	258.65?	259.02?	-	258.31	-	258.05
5^S6	294.11	294.79?	-	-	-	293.77

Note: 2a- according to Nawroozi, 1972.

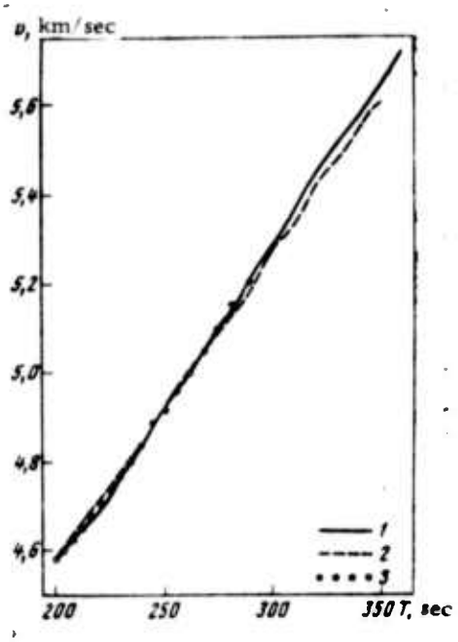

Fig. 3. Dispersion curves determined from R_2, R_4(1), R_4, R_6 (2) and according to Dziewonski, 1971 (3).

Rudnitskiy, V. P. Spectral structure of seismic oscillations and approximate methods for its study. Geofizicheskiy sbornik, no. 59, 1974, 36-45.

Spectral analysis of seismic oscillation was performed and the following conclusions reached:

The spectral analysis of seismic oscillations generated by pulse sources in the solid earth is adequate only as a tool for approximate study (see Fig. 1).

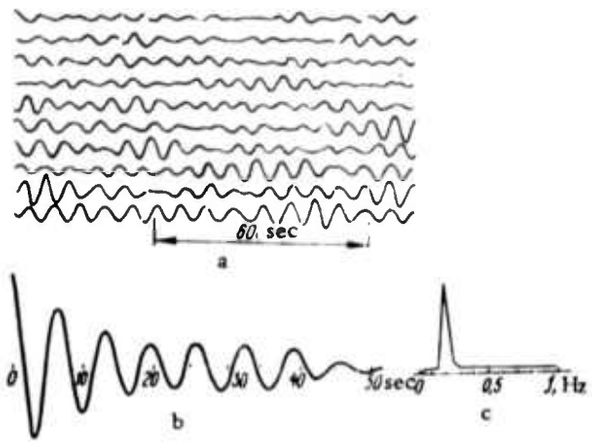

Fig. 1. Example of correlation and spectral analyses of the 4 February 1971 microseismic storm at the Simferopol' station.

a- seismogram; b- autocorrelation function; c- spectral density.

The propagation of seismic body waves in an inhomogeneous earth's crust is accompanied by nonlinear effects which can be identified by means of a coherency function calculated from seismograms of pairs of neighboring stations (see Figs. 2 and 3).

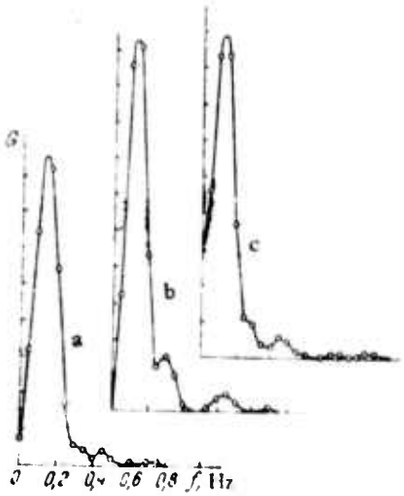

Fig. 2. Spectral densities of the first compressional wave (14-sec interval).

a- Alushta; b- Simferopol'; c- Yalta.

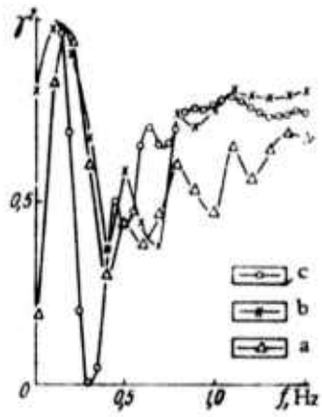

Fig. 3. Coherency functions for three pairs of stations (14-sec interval).

a- Simferopol'-Yalta; b- Simferopol'-Alushta; c- Alushta-Yalta.

The separation of higher harmonics is efficiently accomplished by band-pass filters. Weighting of a filtered function by the unfiltered one improves the estimate of the square of the filtered function and can be used for further tracing of current values of the average energy spectra along seismic profiles.

If quasiharmonic oscillations are generated in the source and the condition $2\Delta\omega_k \leq \omega_0$ is satisfied (where ω_0 is the carrier frequency of the source signal, $2\Delta\omega_k$ band width), an approximate identification of the pulse response of an inhomogeneous medium can be reduced to a series of linear problems by means of band-pass filters.

Soldatov, V. N. Some problems of earthquake signal extraction. AN BelSSR. Izvestiya, no. 6, 1974, 129-130.

The probability of correct detection of seismic signals is studied. The study reduces to an analysis of the signal-to-noise ratio at the output of a receiver in the form

$$\rho = \frac{\{M(\varphi_m)\}^2}{D(\varphi|m)} = \left\{a^2\pi e^{-\frac{\beta^2\pi}{1+\pi\alpha^2}}\right\}\left\{2(1+\pi\alpha^2)\times\right.$$
$$\times\frac{\alpha^2\pi}{2}\left[\frac{1}{\sqrt{1+2\pi\alpha^2}}e^{-\frac{\beta^2}{1+2\pi\alpha^2}}-\frac{1}{1+\pi\alpha^2}e^{-\frac{\beta^2\pi}{1+\pi\alpha^2}}\right]+ \quad (1)$$
$$\left.+\frac{E_n}{2}+\frac{\gamma\sqrt{\pi}}{2\sqrt{1+\gamma^2}}\cdot e^{-\frac{\gamma^2\pi}{2(1+2\gamma^2)}}\right\}^{-1},$$

$M(\varphi_m)$ and $D(\varphi/m)$ are the first and second moments of the normal distribution of $p(\varphi/m)$- a function obtained at the output of the H filter if the output function f(t) contains signal m(t); a is the signal amplitude; E_n is dispersion of white

noise; and

$$\beta^2 = \frac{(\omega_s - \omega_\phi)^2}{\Delta\omega_\phi^2}, \quad \alpha^2 = \frac{\sigma_\omega^2}{\Delta\omega_\phi^2},$$
$$\psi^2 = \frac{(\omega_n - \omega_\phi)^2}{\Delta\omega_\phi^2}, \quad \gamma^2 = \frac{\Delta\omega_n^2}{\Delta\omega_\phi^2}, \qquad (2)$$

The function $\rho(a, \beta, \alpha, \psi, \gamma, E_n)$ was computed accurate to 10^{-7}. Working characteristic curves were plotted which facilitate determining the optimum width and frequency response position for a band-pass filter with a specified probability of correct signal detection.

Molchan, G. M., and V. V. Ratushnyy. Methods of filtering long-period signals over short time intervals. IN: Vychislitel'naya seysmologiya, no. 7, Moskva, Nauka, 1974, 130-160.

A comprehensive account is given of filtering methods using exponential smoothing filters with transfer functions $K_T(p) = 1 + pT)^{-1}$ which were developed for marine gravimetry. The accuracy of measuring a smoothed function at random points is analyzed. Numerical examples are given illustrating the design of filters in the form $K = \sum_{i=1}^{n} \mu_i K_{T_i}$, $T_i \leq T_0$ and measurement of a smoothed function at extrema of a centered function (1-K)s(t).

It is concluded that efficient low-frequency filters can be designed, combining filters of exponential smoothing by multiplication and addition. Measurement of the function at zeros of an auxiliary function with zero-average value can be efficient only if the measured and auxiliary functions are sufficiently well correlated. The highest accuracy is attained if zeros of the auxiliary function are determined by a vertical window-type operator. Measurements at random points over long time intervals are equal to measurements at uniformly spaced points with the same density in the sense of an asymptotic equality of depressions of the average error of all measurements.

Borkovskiy, G. M., A. A. Drozdov, V. M. Kreysberg, and A. A. Tsukanov. Device for reproduction of digital seismic information. Otkr, izobi, no. 20, 1974, 115. (Translation)

The device described by this patent contains a analog-code converter, a dynamic-range reproduction circuit, channel selector, continuous analog signal shaper, and recorder. To improve economy and provide identical channel control, between the output of the dynamic range reproduction circuit and the imput of the channel selector, an automatic gain control system (AGC) has been added for multichannel seismic information in a single amplifying channel. In the AGC, the output of the reproduction circuit is connected to the amplification input of a common amplifier with a regulated gain coefficient, whose output is connected to the input of the amplifier of the AGC loop of the common amplifier. This amplifier is connected through a series connected phase shifter, rectifier, and filter to the control input of the common amplifier which is connected to the input of the channel selector. The outputs of any two opposing end channels and of any central channel of the continuous analog signal shapers are connected to the input of a mixer. The mixer output is connected to the amplifier input of AGC loop. To the second inputs of the phase shifter, a switchable splitter is connected, the first input of which is connected to the output of a multivibrator, while the second input of the splitter is connected to the output of a time relay. The time-relay input is connected to the circuit providing the detonation time mark.

Borkovskiy, G. M., A. A. Drozdov, and V. M. Kreysberg. Method of visualization of multichannel digital seismic information. Otkr izobr, no. 20, 1974, 115. (Translation)

Digital information, compressed in time, is converted into analog form with subsequent channel distribution. This method is distinguished

by the amplification of compressed analog seismic signals employed for the purpose of compressing the dynamic range in the case of identical channels and to preserve dynamic distinctiveness of the records. The amplification coefficient is changed proportionally to the summed energy of the signals.

Gur'yanov, V. M. Breakdown of a seismic wave field into travelling waves. IN: Sb. Primeneniye TsVM i sredstv vychisl. tekhn. v geol. i geofiz. Saratov, 1974, 3-18. (RZhMekh, 11/74, #11V837) (Translation)

The theory of the breakdown of summary seismic wave field into its component travelling plane waves was developed on the basis of the solution of the Lamé equations for an nonhomogeneous isotropic elastic theory with ray approximation. This approach is associated with a study of characteristics of spectral functions which are obtained by applying a two-sided integral Fourier transform to the expression for the displacement field for an nonhomogeneous elastic medium. It was shown that the amplitude-frequency characteristics of seismic waves recorded by a linear receiver arrangement satisfy a system of integral equations of the Fredholm type, which can be solved by an approximate method. Coefficients of the approximate solutions are found from the condition of functional minimization on the basis of the least squares method.

The basic principles of the theory developed are illustrated by an example of an approximate breakdown of summary seismic field into waves with equal time-distance curves. It was pointed out that it is sufficient to have a minimum volume of experimental information: time-distance curve for first arrivals and time distance curve for trailing edges; information on the shape and intensity of interference waves is not needed.

Lander, A. V. Methods for interpretation of results of frequency-time analysis. IN: Vychislitel'naya seysmologiya, no. 7, Moskva, Nauka, 1974, 279-315.

A comprehensive account of frequency-time analysis of seismological data, fundamentals of the analysis of body and surface seismic waves, as well as a description of the analysis techniques are given. The following is a summary of the study.

The physical meaning of the results of frequency-time analysis (FTA) depends strongly both on the shape of the signal and the techniques of the analysis applied. It varies widely depending on the selection of filters. Therefore, the selection of filters is the most important step in FTA. The main problems - extraction of signal and measurement of its parameters are solved simultaneously by FTA. It is not an optimum method, for the signal extraction of parameter measurements, and it has limited possibilities. The best signal extraction may be accompanied by poor parameter measurements and vice versa. In every real situation, a compromise should be selected. The selection of filters is determined by the problem to be solved, as well as by the type of signals studied. A possible way to improve methods of FTA is a preliminary transformation of the signal into a form for which the conflict between the extraction of a signal and measurement of its parameters is less severe. The great advantage of FTA is that it requires no prior information on the signal.

3. Explosion Seismology

Kostyuchenko, V. N., and V. N. Rodionov.
Radiation of seismic waves during powerful underground explosions in solid rock.
Fizika Zemli, no. 10, 1974, 65-73.

An estimate is made of parameters of seismic waves radiated by underground explosions, based on an approximate model of underground explosions in solid rock as developed by Radionov et al., 1968 and Radionov et al., 1971. The estimates are compared to experimental data on underground nuclear explosions in rock salt and granite.

The results of calculations of the maximum displacement and velocity of compressional waves from explosions in rock salt and granite are shown in Figs. 1 and 2.

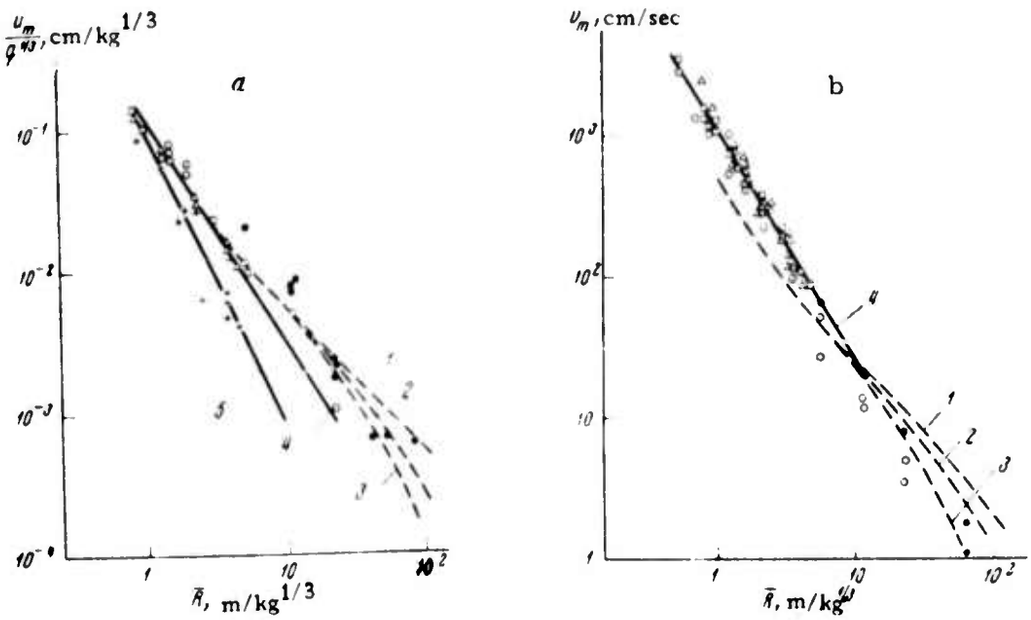

Fig. 1. Maximum displacement (a) and velocity (b) in compressional waves from explosions in salt.

Curves 1, 2, and 3- calculations for absorption decrement D = 0, 0.05, and 0.1, respectively; Curve 4- average from measurements in the interior and at the surface of the rock mass (open and solid circles, respectively); Curve 5 and crosses - residual displacements from Salmon explosion. (circles - Gnome data; triangles- Salmon; squares - USSR)

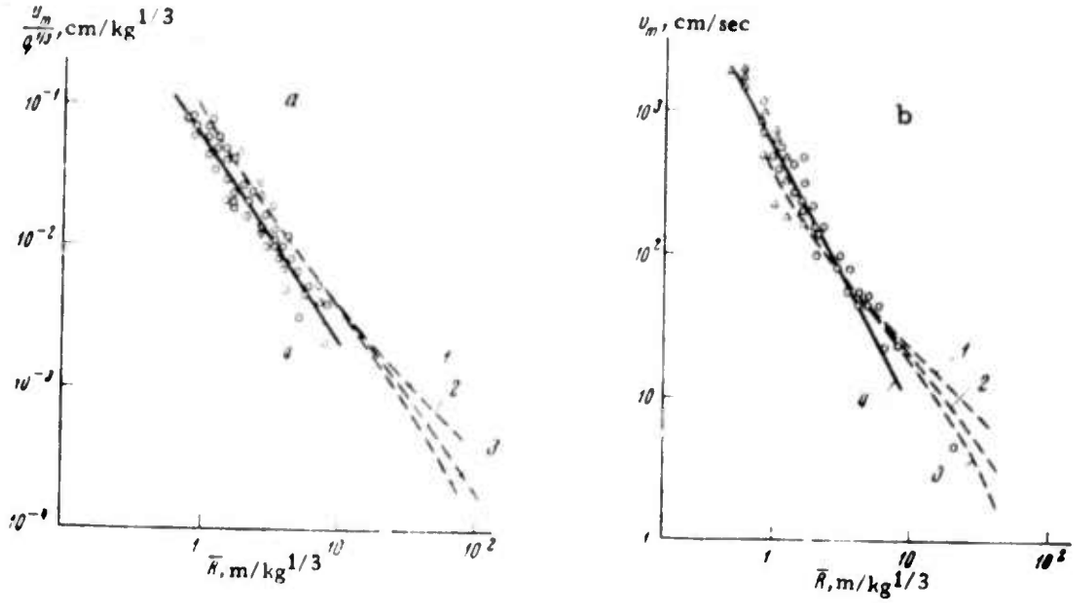

Fig. 2. Maximum displacement (a) and velocity (b) in compressional waves from explosions in granite.

Curves 1, 2, 3- calculations for D = 0, 0.05, and 0.1, respectively; Curve 4- average from measurements in the interior of the rock mass (open circles- Sahara data; triangles - Hardhat and Shoal).

The maximum radius of the elastic zone a_m, maximum displacement at the boundary of the elastic zone u_0, and characteristic radiation time T_0 were calculated to be: $a_m/q^{1/3} = 1$ m/kg$^{1/3}$, $u_0/q^{1/3} = 0.1$ cm/kg$^{1/3}$, $T_0/q^{1/3} = 1$ msec/kg$^{1/3}$ for salt ($\rho = 2.2$ gr/cm^3, $V_P = 4.4$ km/sec, $\sigma_*/\rho V_P^2 = 10^{-3}$); and 0.87 m/kg$^{1/3}$, 8.7×10^{-2} cm/kg$^{1/3}$, and 0.64 msec/kg$^{1/3}$ for granite ($\rho = 2.7$ gr/cm^3, $V_P = 5.5$ km/sec, $\sigma_*/\rho V_P^2 = 10^{-3}$).

Measured and calculated time dependencies of displacements from explosions in salt and granite are shown in Fig. 3 and Fig. 4, a.

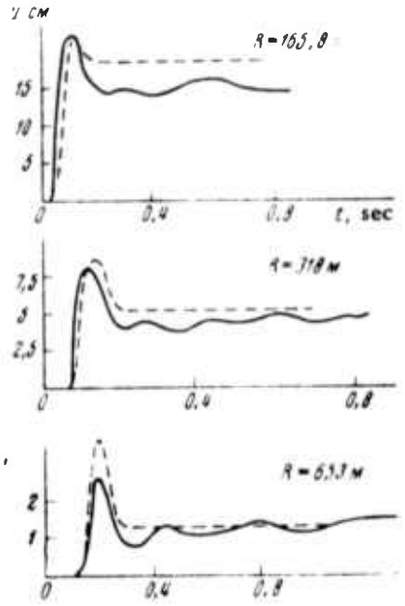

Fig. 3. Measured displacement fields from Salmon explosion (solid lines) and calculated values (dashed lines).

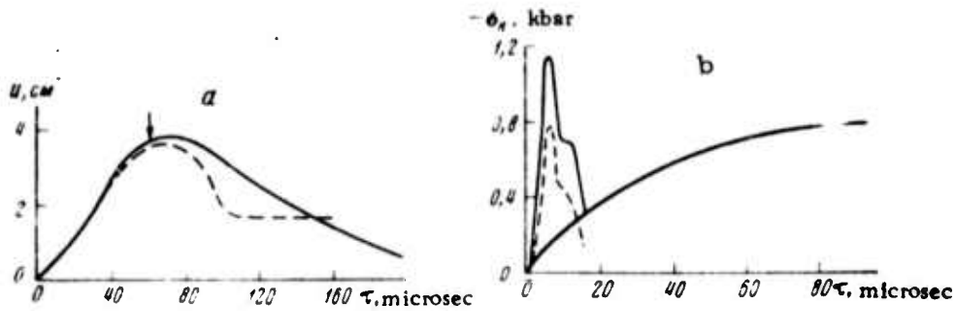

Fig. 4. Displacement (a) and radial stress (b) from Hardhat explosion and calculated values.

a. solid line - measurements; dashed line - calculations.
b. thin solid line - measurements at R = 120 m; dashed line - calculations for R = a_m = 150 m according to $\sigma_R = 1/R^n$ (n = 1.5-2); thick solid line - calculations according to $-\sigma_R(\tau) = \sigma_* (1-e^{-d\tau})$, where $\alpha = 2.2/t_m$, $\sigma_* = 10^{-3}\rho V_p^2$ = 800 b.

It is pointed out that a quasistatic approximation adopted in the analysis of the last stage of explosion development can describe adequately only radiation in the low-frequency range, as illustrated in Figs. 4 b and 5. Figure 5 gives the spectrum of

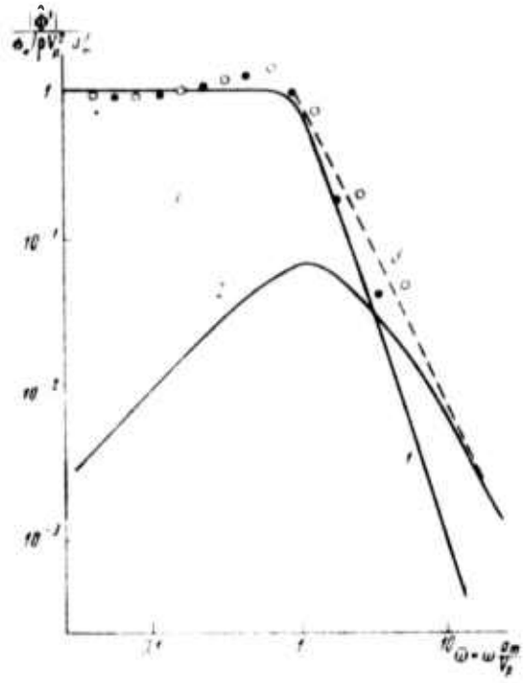

Fig. 5. Spectrum of signals radiated during explosions.

Open circles - Gnome data; solid circles - Hardhat; Curve 1 - calculations in quasistatic approximation; Curve 2 - calculations for head waves; Curve 3 - calculations by $|\hat{\Phi}'| = 0{,}8 \frac{\sigma_1}{\rho} \frac{a_m}{\omega^2}$.

the derivative of potential $|\hat{\Phi}'|$ which at large distances represents the spectrum of displacement in compressional waves. Calculations of $|\hat{\Phi}|$ were made assuming $\gamma = 0.5$, $\alpha\, a_m/V_P = 1$ and $-\sigma_R(\tau) = \sigma_*(1-e^{-\alpha\tau})$, $\alpha = 2{,}2/t_m$, where $\alpha = 2.2/t_m$ in a quasistatic approximation and $\sigma_R = \sigma_1 e^{-\alpha_1 \tau}$, where $\alpha_1 = 10\,\alpha$, $\sigma_1 = \sigma_*$ for head waves. The figure illustrates that for $\bar{\omega} \leq 1$-2, the quasistatic approximation sufficiently well describes the spectral amplitude of waves, while at high frequencies, calculations for head waves give better results.

Zel'manov, I. L., V. N. Kologrivov, A. A. Krasavin, V. I. Kulikov, V. V. Pedanov, and A. M. Tikhomirov. Study of seismic effect of an explosion on a transparent model. Fizika Zemli, no. 10, 1974, 80-91.

A description is given of the techniques, method, and results of a model study of seismic effects of explosions. The results were compared to those obtained from data on nuclear and chemical explosions in solid rock.

The models used were fabricated from K-8 and TF-5 optical glasses and aluminum-potassium alum ($KA\ell(SO_4)_2 \cdot 12H_2O$). Mechanical and physical properties of materials used for the models are given in Table 1.

Table 1

Material	ρ, gr/cm^3	E, kg/cm^2	ν	C_ℓ km/sec	C_ℓ km/sec	σ kg/cm^2	n
K-8 glass	2.52	$8.4 \cdot 10^5$	0.19	6.06	3.74	$7\text{-}10 \cdot 10^3$	1.516
TF-5 glass	4.77	$5.8 \cdot 10^5$	0.22	3.71	2.22	$6.5 \cdot 10^3$	1.755
Aluminum	1.75	$2.25 \cdot 10^5$	0.25	3.93	2.26	150	1.456

Note: σ is compressive strength, n refractive index.

The explosions were simulated by a plasma focus produced by focusing single-pulse radiation of a Q-switched ruby laser in the models, as shown in Fig. 1. The parameters of the laser are as follows: pumping energy 3kj; pulse energy 1j; pulse half-width 20 nsec; and beam diameter, about 10 mm. Energy density of the "laser" explosion was $\approx 1.8 \times 10^4$ j/cm^3.

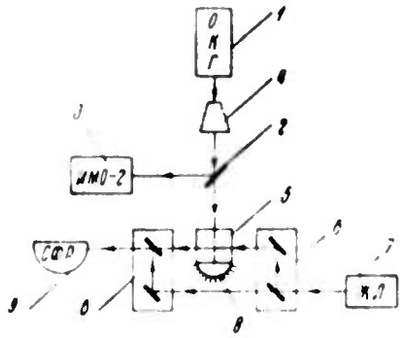

Fig. 1. Experimental Set-Up.

1 - laser; 2 - sloping plate; 3 - power-level indicator; 4 - telescope; 5 - target; 6 - Mach-Zehnder interferometer; 7 - liquid-dye laser; 8 - spherical mirror; 9 - high-speed camera.

The parameters of compressional waves were determined by the interference method. Interferograms were processed by the "travelling wave" method. An example of interferogram processing of the explosions in TF-5 is shown in Fig. 2.

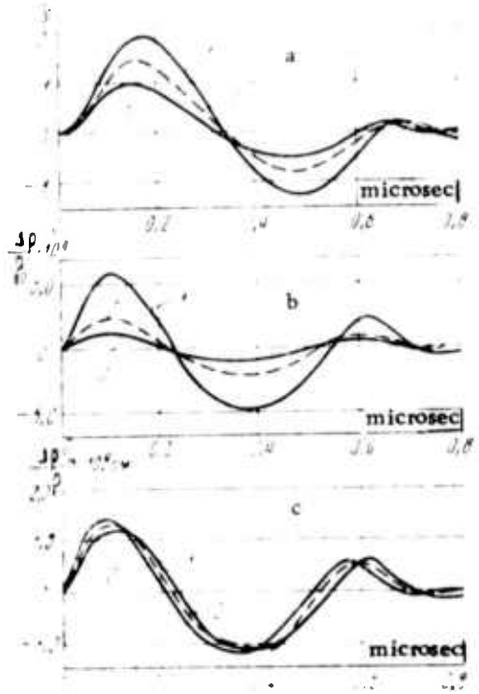

Fig. 2. Displacement of the central band (a) density diagrams (b) and second derivatives of displacement potential (c).

Curves 1, 2, and 3 represent 2.27, 5.95, and 11.60 mm offsets of the camera slit from the explosion center, respectively.

The results of model studies of explosions in solids, as well as their comparison with results obtained from data on nuclear and chemical explosions in rock, are given in Figs. 3-6 and Tables 2-4.

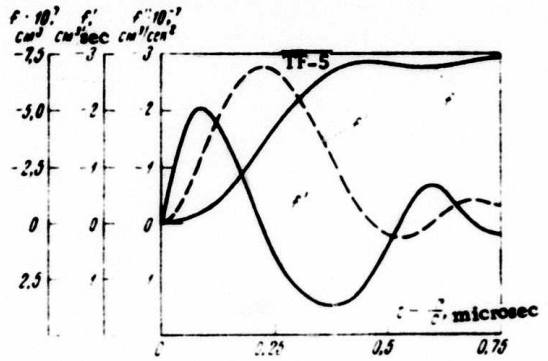

Fig. 3. Displacement potential and its derivatives for explosion in TF-5 (energy 1 J).

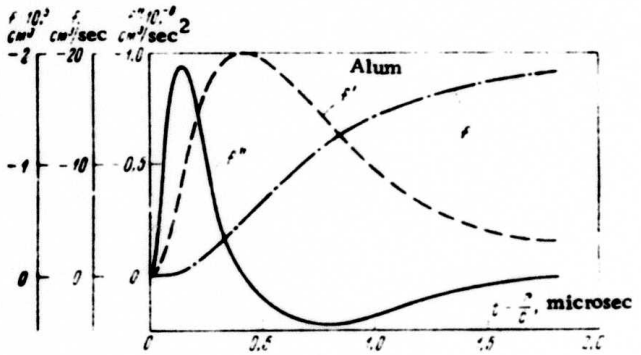

Fig. 4. Displacement potential and its derivatives for explosion in alum (energy 1 J).

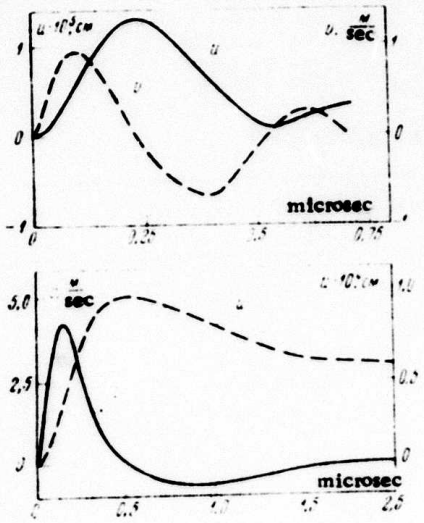

Fig. 5. Diagrams of velocity and displacement in TF-5 (a) and alum (b) at 6 mm from the explosion center.

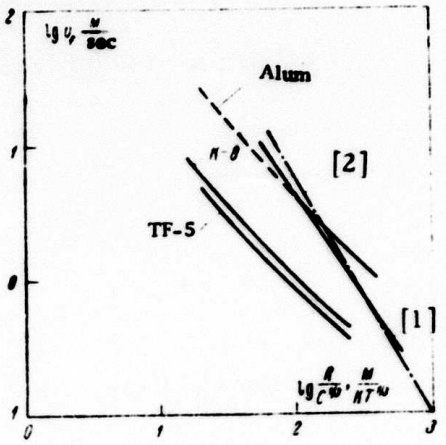

Fig. 6. Maximum mass velocity for laser and nuclear explosions (1- after Derlich, 1970; 2- Trembly and Berg, 1966).

Table 2

Radius of shattered and fractured zones

Medium	Explosion	kg/cm^2	r_1 m/kT$^{1/3}$	r_2 m/kT$^{1/3}$
K-8 glass	Laser	$7\text{-}10\cdot10^3$	8.8	20.5
TF-5 glass	-11-	6500	5.74	15.8
Alum	-11-	160	39	130
Granite	Nuclear (Derlich, 1970)	2000	10.2	27
(?)	-11- (Kedrovskiy et al., 1970)	-	20-30	50-70
Rock salt	Chemical (Rodionov et al., 1967)	400-600	33	-
Sodim thiosulphate	-11-	160-200	44	-

Table 3

Seismic yield of laser and nuclear explosions

Material	Portion of explosion yield e, %
K-8	0.09
TF-5	0.12
Alum	0.92
Tuff (Rodionov et al., 1971)	0.2-0.3
Granite (Trembly and Berg, 1966)	0.7-2.0

Table 4

Ejecta volume for laser and cavity volume for nuclear and chemical explosions

Material	Explosion	V, m^3/kT	V, m^3/kT
K-8 glass	Laser	28.3	-
TF-5 glass	"	38.3	-
Alum	"	1250	-
Granite	Nuclear (Derlich, 1970)	-	1640
Granite	" (Kedrovskiy et al., 1970)	-	4000-14000
Rock salt	" (Boardman, 1970)	-	3500-7900
Rock salt	" (Kedrovskiy et al., 1970	-	5600-100000
Rock salt	Chemical (Rodionov et al., 1967)	-	5450
Sodium thiosulphate	"	-	12700

Vovk, A. A., A. V. Mikhalyuk, and I. V. Belinskiy. Producing underground cavities by a confined explosion in an isotropic rock mass. PM, v. 10, no. 9, 1974, 53-59.

Formulas are developed for cavity radius produced by an underground explosion, taking into account the behavior of rocks under blast load, which are suitable for underground engineering applications. The results of experiments with uniaxial dynamic compression of rocks without lateral expansion are given in Fig. 1. The calculating model is shown in Fig. 2.

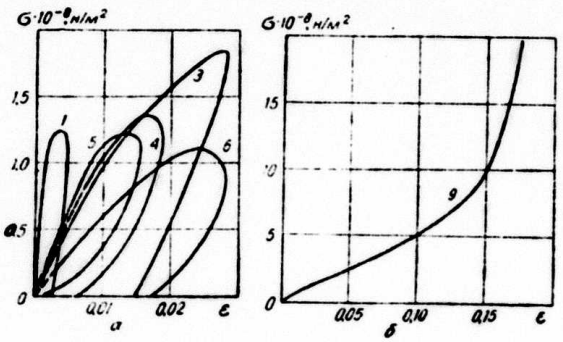

Fig. 1.

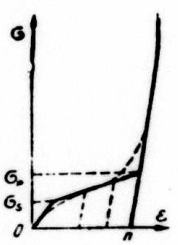

Fig. 2.

The results of calculation and their comparison with experimental data are given in the table.

No.	Rock	Q, kg	r, m	$k \cdot 10^{-8}$ n/m^2	μ	R_C	R_e	$R_e - R_c / R_c$, %
1	Sandy loam	0.20	0.031	21.4	2.6	9.4	9.37	-0.3
2	Dusty limestone	0.20	0.031	130.0	2.0	5.9	6.40	8.5
3	"	0.18	0.030	130.0	2.0	5.9	6.30	6.8
4	"	0.18	0.030	130.0	2.0	5.9	5.70	-3.4
5	Concrete	0.12	0.026	13.3	1.5	2.1	1.93	-8.1
6	Sandstone	0.10	0.024	150.0	2.0	3.1	2.99	-3.5
7	Granite	0.12	0.026	580.0	2.1	2.01	1.90	-5.0
8	Granite (Hardhat event)	$4.8 \cdot 10^6$	8.92	123.0	1.6	2.05	2.15*	4.9
9	Granite (Shoal event)	$12.2 \cdot 10^6$	12.20	123.0	1.6	2.05	2.10*	2.4
10	Granite (Piledriver event)	$56.0 \cdot 10^6$	20.30	123.0	1.6	2.05	1.96*	-4.4

Note: * - according to Higgins, 1970.

Koryavov, V. P. Forerunner effect on motion in the near-explosion zone. Fizika Zemli, no. 10, 1974, 74-79.

The results are presented of an analysis of the effect of an elastic medium's strength on elastic energy, cavity dimension, and fracture zone dimension, resulting from a powerful underground explosion. In the formulation of the problem, elastic waves are radiated at the front of destruction of an elastic medium, i.e., its conversion into a fluid medium. The fluid medium is described by equations of state obtained from shock adiabatics for solids (Koryavov and Vilenskaya, 1968). In the present calculations, a change in the conditions at the shock wave front is introduced. All calculations are made for fracture condition in the form

$$p_e - p_\theta = \alpha,$$

where p_e and p_θ are radial and azimuthal stress, respectively in the elastic wave in front of the shock wave. It is assumed that α = 5 kb, c_ℓ = 5.44 km/sec, σ = 0.27, and other parameters are the same as in the above-mentioned work.

The results of calculations are shown in Figs. 1-3. A comparison of the present results with experimental and theoretical values reported by other authors is given in the table.

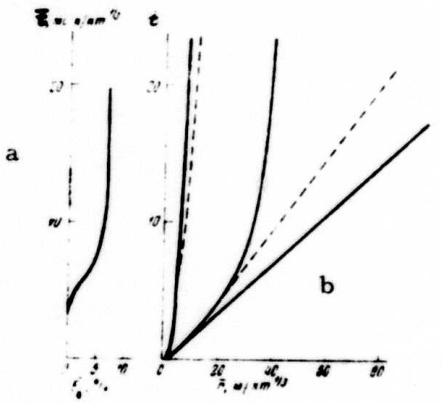

Fig. 1. Time variation of elastic energy outflow at shock front (a) and propagation of shock front, forerunner, and cavity boundary (b).

Dashed lines - propagation of shock front and cavity boundary without accounting for elastic waves.

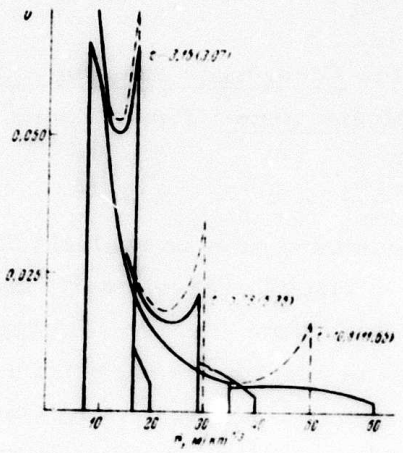

Fig. 2. Mass velocity profiles (D_o = 3.7 km/sec) considering (solid lines) and not considering (dashed lines) elastic forerunner.

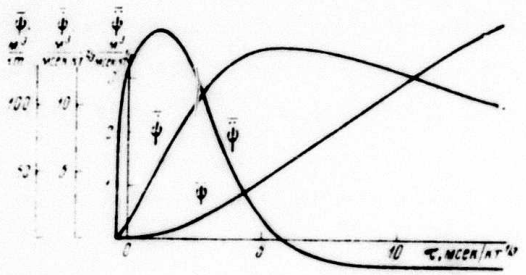

Fig. 3. Elastic potential and its derivatives reduced to a detonation energy of 1 kt.

Author	Medium	Cavity radius, $m/kt^{1/3}$	Fracture zone radius, $m/kt^{1/3}$	Elastic zone radius, $m/kt^{1/3}$	Elastic wave energy, %	Elastic potential $\psi_\infty \cdot 10^{-3}$, m^3	ψ_{max}/ψ_∞	Density ρ_o, gr/cm^3	Compressional wave velocity C_l, km/sec	Shear wave velocity C_t, km/sec	Bulk modulus K, kb	Shear modulus G, kb	Poisson ratio	Mie-Gruneisen coefficient Γ	Vaporization pressure P_e, mb	Plastic flow criterion Y, kb
Butkovich	Granite	-	41.5	175	-	-	-	2.67	5.44	3.05	361	315	-	1.0	2.14	1-10
Holzer (exp.)	Granite	-	-	-	-	-	-	2.67	5.44	3.05	361	315	-	1.0	-	1-20
	Salt	-	-	-	-	-	-	2.24	4.55	2.16	342	104	-	1.4	-	0.05-0.5
	Tuff	-	-	-	-	-	-	1.89	2.4	1.64	66	33	-	1.5	-	1-10
Haskell (exp.)	Granite	-	-	-	3.68	2.5	1.75	-	-	-	-	-	-	-	-	-
	Salt	-	-	-	4.9	4.4	1.5	-	-	-	-	-	-	-	-	-
	Futt	-	-	-	1.18	5.12	1.0	-	-	-	-	-	-	-	-	-
	Aluminum	-	-	-	0.11	0.42	2.8	-	-	-	-	-	-	-	-	-
Mueller	Granite	-	-	206	1.8	-	-	-	-	-	-	-	-	-	-	-
	Salt	-	-	172	5.8	-	-	-	-	-	-	-	-	-	-	-
	Tuff	-	-	106	6.1	-	-	-	-	-	-	-	-	-	-	-
Cherry, Petersen	Granite	11.9	52.5	-	-	2.0	1.0	2.67	-	-	-	-	0.28	-	-	7.5
	Granite	5.89	46.5	-	-	-	-	2.67	5.44	3.05	361	315	-	1.0	-	1-20
Higgins (exp.)	Granite	11.2	-	-	-	-	-	2.65	4.6; 5.5	-	567	-	0.28	-	-	7.5 (dry); 1.5 (wet)
	Salt	12.0	-	-	-	-	-	2.24	4.5	-	260	-	0.26	-	-	1.0
	Tuff	14.0	-	-	-	-	-	1.9	3.0; 3.7	-	50; 90	-	0.25	-	-	3.0
Franch (exp.)	Granite	7.3	26	71	-	2.5	1.6	2.63	-	-	550	274	-	-	-	-
Rodionov et al.	Granite	-	-	120	-	-	-	-	-	-	-	-	-	-	-	0.52
	Salt	-	-	128	-	-	-	2.15	4.5	2.4	-	-	0.25	-	-	0.4-0.6 (uniaxial pressure)
	Tuff	-	-	100	0.2	-	-	-	-	-	-	-	0.32	-	-	-
Batalov et al.	Salt	9; 11	-	-	-	-	-	2.16	-	-	-	-	0.33	1.0	-	0.4; 0.2
Grigoryan, Pechenskiy	Granite	11.2; 10	82	124; 144	-	2.5	1.7	2.67	5.4	-	-	314	0.16	0.12	1.8	18
Present Results		9	41	-	7.3	-	-	2.67	5.4	-	-	-	0.27	1-1.5	-	5

4. General

Sinitsyn, A. P. Seismic effect from several sources. AN SSSR. Trudy Instituta fiziki Zemli, no. 16, 1974, 65-72.

An analysis is made of seismic effect due to a point force suddenly applied to the surface at an elastic halfspace in the case of: 1) two fixed sources; 2) two moving sources approaching each other; and 3) two pairs of moving sources, two approaching each other and two receding from each other.

The wave patterns in the first case are shown in Figs. 1 and 2. In the inner zone of the halfspace (between the sources), seismic effect is amplified due to the interaction of waves. The collision area (shaded area in Fig. 1) can be considered as an additional source, twice as strong as the individual sources. The wave pattern in the outer zone is shown in Fig. 2. The seismic effect in this zone is amplified due to the "imaginary" source in the inner zone, and exceeds the simple summary effect of two sources by a factor of 1.5 (see Fig. 3).

In the second case which is illustrated in Fig. 4, the two sources approach each other at supersonic speed. Due to interaction of waves, compressional wave reflection occurs which approximates reflection from a fixed obstacle. Thus, the amplitude of reflected waves is twice as large as the amplitude of incident compressional waves.

In the third case, which is illustrated in Fig. 5, the wave pattern in the inner zone is the same as in the second case. In the outer zone, three different compressional waves occur: direct waves from two pairs of sources and reflections from the collison plane which is formed in the inner zone. The seismic effect in the outer zone exceeds the simple summary effect of two pairs of sources by 60-70% (see Fig. 6)

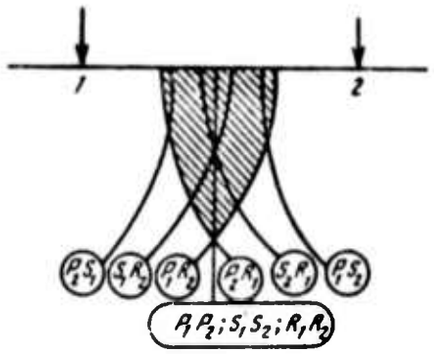

Fig. 1. Collision of waves from two sources.

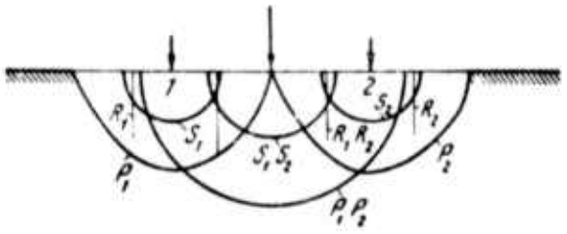

Fig. 2. Generation of an imaginary source.

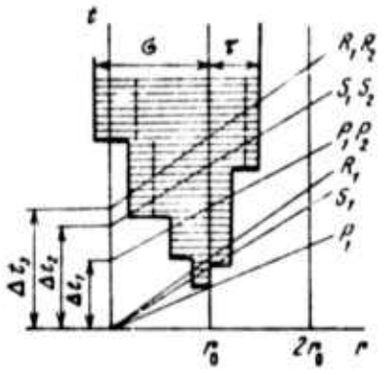

Fig. 3. Diagram of wave network

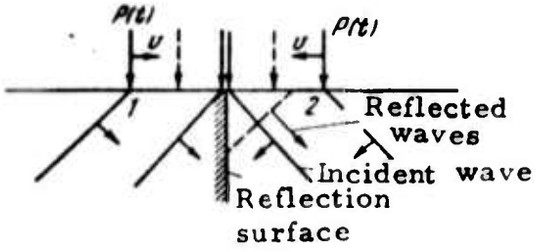

Fig. 4. Waves resulting from two moving sources.

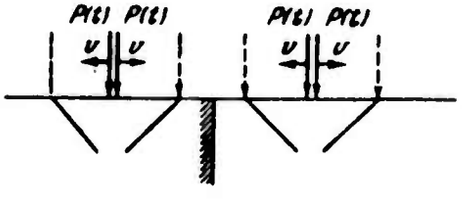

Fig. 5. Waves resulting from two pairs of moving sources.

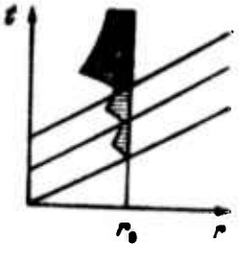

Fig. 6. Diagram of wave network.

AN SSSR. Institut fiziki Zemli. Apparatura i metodika seysmometricheskikh nablyudeniy v SSSR (Equipment and methods for seismometric observations in the USSR) Moskva, Izd-vo Nauka, 1974, 242 p.

This book reviews fundamentals in the theory of seismometer channels, and the basic types of seismic, recording, and control instrumentation used in permanent observatories, field stations, and engineering sites are described. Methods and equipment used at permanent and temporary observatories are reviewed. The table of contents of this book is as follows:

Savarenskiy, Ye. F., and G. L. Kosarev. Effect of crustal structure beneath a seismological station on motion in compressional waves. Fizika Zemli, no. 10, 1974, 113-120.

An analysis is made of the dependence of apparent angles of emergence of compressional seismic waves at a seismological station on local crustal structure, real angles of emergence at the crustal base and frequency of oscillations as well. An attempt is made to determine the parameters of a layered crust from spectra of apparent angles of emergence.

Computer calculated values of vertical and horizontal components of the amplitude of the motion of the earth's surface as recorded by a long-period seismograph for a single-layered crust overlaying a half-space and for different incident pulses are shown in Figs. 1 and 2. Observed and calculated seismograms for a multi-layered crust overlaying a half-space are shown in Fig. 3 and 4. A comparison between seismograms calculated for a single-layered crust overlaying a single- and multi-layered upper mantle is given in Fig. 5. The model of a 1000 km-thick multi-layered upper mantle (several hundred 2-5 km-thick layers) used in the calculations was based on the velocity distribution for shear waves typical of continental platforms. Densities were calculated by the formula $\rho_k = 0.763 + 0.328\, a_k$ (where a is the velocity of compressional waves).

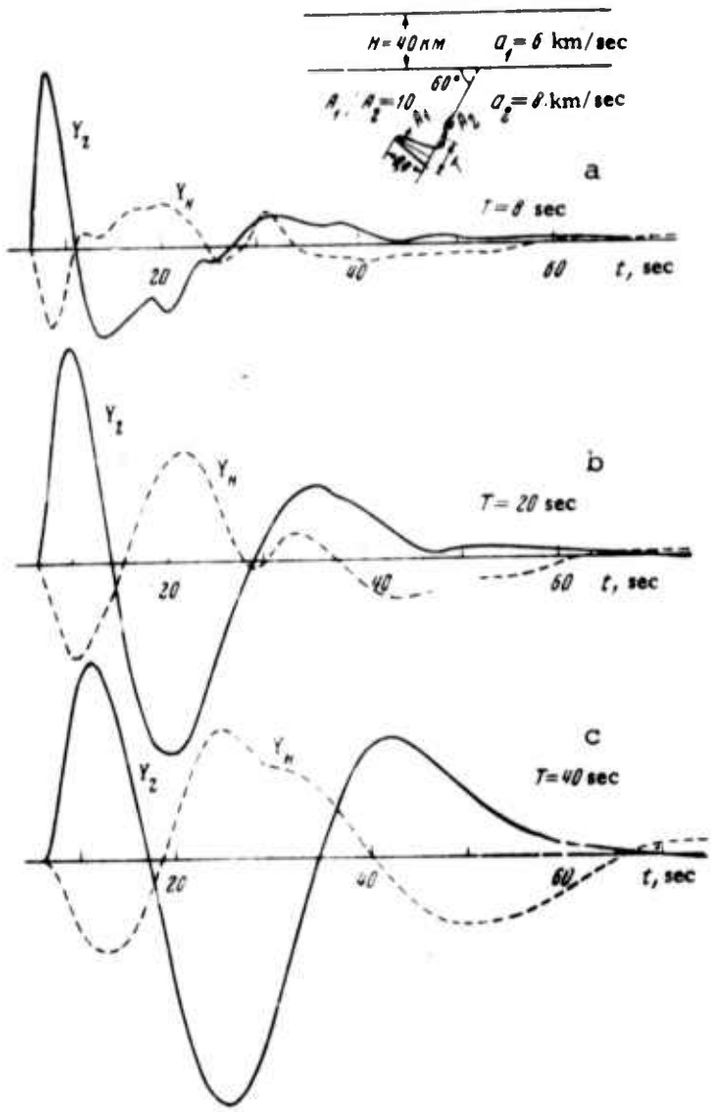

Fig. 2. Motions in compressional waves at the surface of a single-layered crust as recorded by a long-period seismograph for different periods of incident pulse.

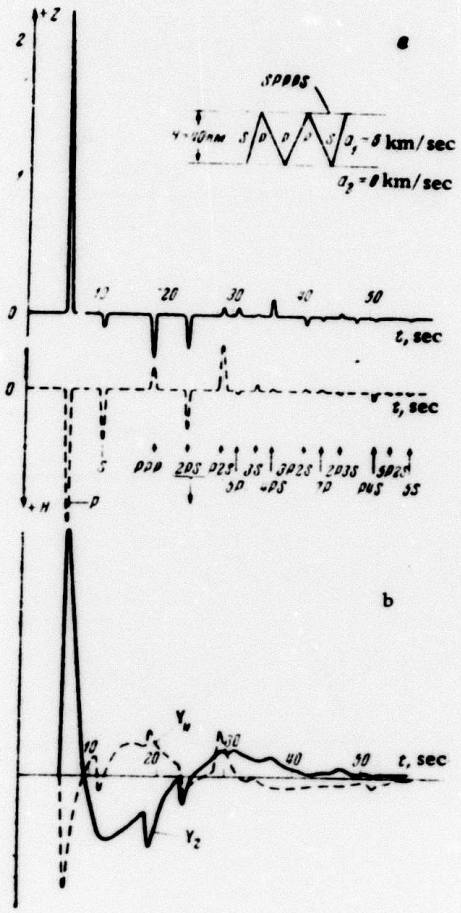

Fig. 1. Motions in compressional waves at the surface of a single-layered crust (bell-shaped incident pulse).

a - real motions; b - record by a long-period seismograph (T_S = 30 sec; T_g = 100 sec, D_S = 1, D_g = 0.5)

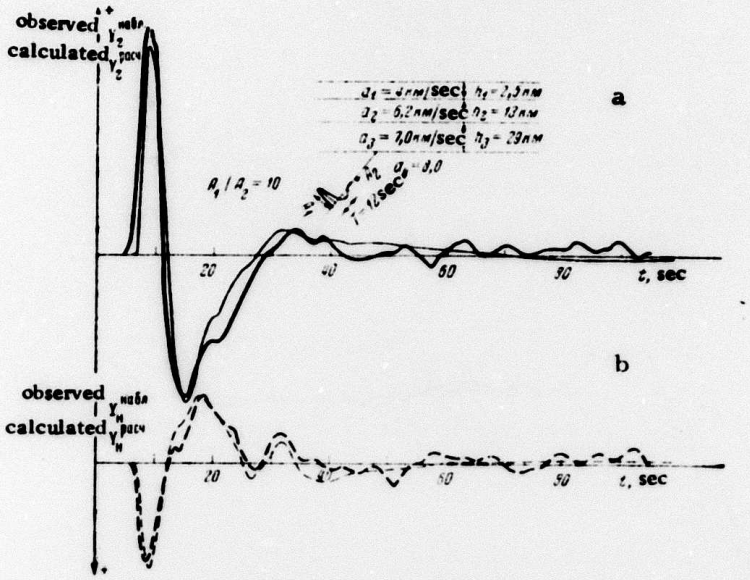

Fig. 3. Calculated (thin line) and observed (thick line) seismograms of compressional waves from the 27 May, 1970 earthquake in the Bonin Islands and observed at the Obninsk station.

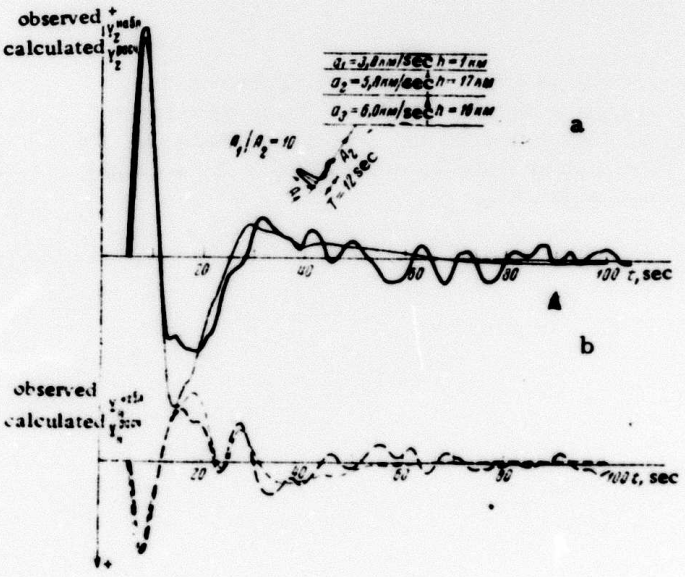

Fig. 4. Calculated (thin line) and observed (thick line) seismograms of compressional waves from the 24 March, 1967 earthquake in the Malay archipelago and observed at the Yuzhno-Sakhalinsk station.

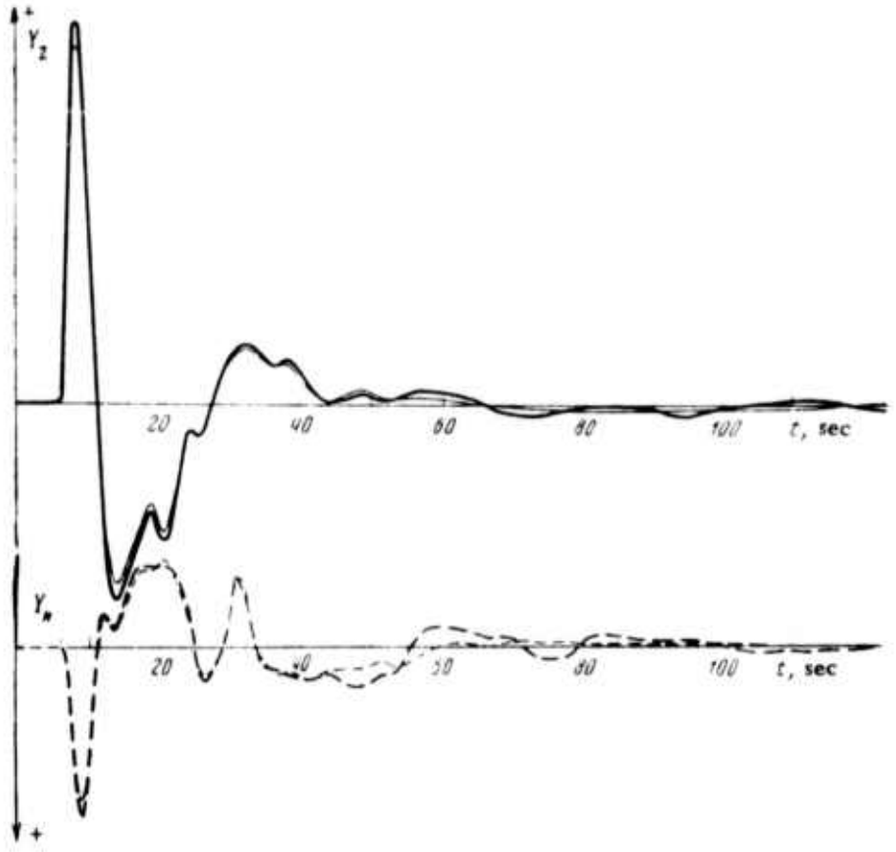

Fig. 5. Motions in compressional waves at the surface of a single-layered crust overlaying a single-layered (thin line) and multi-layered (thick line) upper mantle as recorded by a long-period seismograph.

Crustal parameters and incident pulse the same as in Fig. 2.

Sobolev, G. A., and L. B. Slavina. Rapid changes in electric and seismic properties of the medium in a seismically active region. DAN SSSR, v. 215, no. 5, 1974, 1101-1104.

Data on rapid changes in electrotelluric field and velocities of compressional and seismic shear waves from earthquakes with $K \geq 8$, $\Delta \leq 150$ km observed in the Kamchatka region were analyzed using uniform processing techniques. The observation stations and distribution of epicenters for strong earthquakes are shown in Fig. 1.

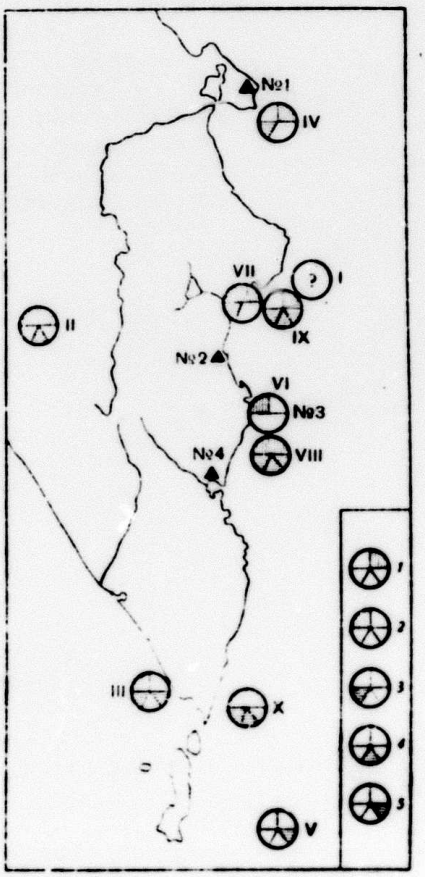

Fig. 1. Positions of observation stations and epicenters of strong earthquakes. Shading indicates that prior to the earthquakes there were observed peaks in: 1- $|\overline{\Delta V}|^2$ at No. 1 Station; 2- $|\overline{\Delta V}|^2$ at No. 3; 3- $|\overline{\Delta v_p/v_s}|^2$ at No. 2; 4- $|\overline{\Delta v_p/v_s}|^2$ at No. 3; 5- $|\overline{\Delta v_p/v_s}|^2$ at No. 4.

Variations in the electrotelluric and elastic terrestrial fields in the Kamchatka region during 1972-73 are illustrated in Fig. 2.

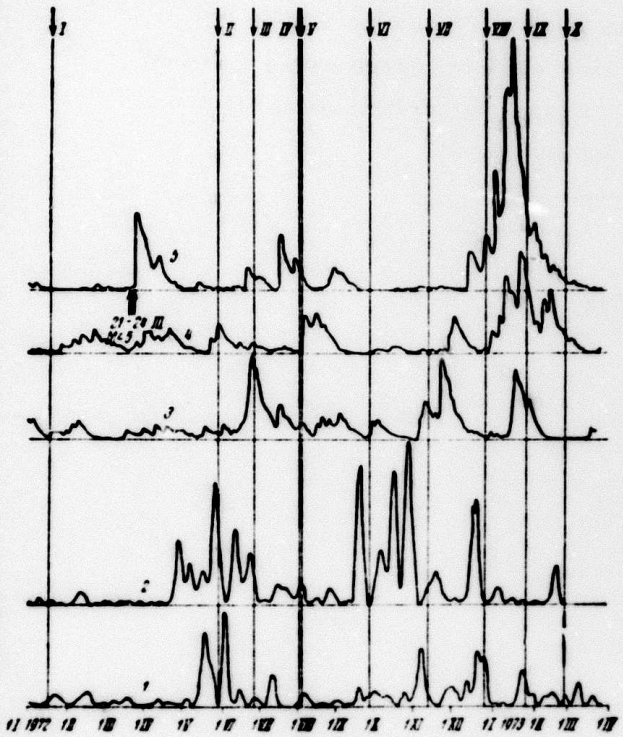

Fig. 2. Variations of $\overline{|\Delta V|^2}$ at No. 1 and No. 3 stations (1, 2) and $\overline{|\Delta v_p/v_s|^2}$ at the No. 2, No. 3, and No. 4 stations (3, 4, 5).

Earthquakes:

I- 18 January 1972, M = 5.4;
II- 25 May 1972, m_{pv} = 6.2;
III- 26 June 1972, m_{pv} = 6.1;
IV - 2 August 1972, M = 5.9;
V - 4 August 1972, M = 6.7;
VI- 27 September 1972, M = 5.1;
VII- 10 November 1972, m_{pv} = 5.2;
VIII- 25 December 1972, M = 5.6;
IX- 25 January 1973, M = 5.0;
X- 28 February 1973, M = 7.4.

It was found that numerous strong earthquakes are preceded by rapid changes in electrotelluric field and the ratio between velocities of compressional and seismic shear waves. These changes were not strictly simultaneous over the entire region, but were observed at rather large distances from the subsequent earthquakes.

Yanovskaya, T. B. **Determining depth of the core boundary from travel times of PcP waves and time-distance curve of P waves.** IN: Sb. Teor. i vychisl. geofiz. No. 2. M., 1974, 76-90. (RZhMekh, 11/74, #11V828). (Translation)

A method is proposed for determining the radius of the earth's core and the velocity gradient in the layer above the core, using data on travel times of PcP waves and time-distance curve of P waves. The formulas for transformation of time-distance curves of refracted waves into time-distance curves of reflected waves were used. It was shown that the ambiguity in time-distance curves of P waves at a distance of about 20° (loop, shadow zone) has practically no effect on time-distance curves calculated for PcP waves. The core radius r_i and the velocity gradient dv/dz were estimated using previously published data (see Herrin E., Tucker W., Taggart J., Gordon D. W., Lobdell J. L., Bull. Seismol. Soc. Amer., 1968, 58, No. 4, 1273-1291). A 90%- confidence region for calculated parameters was outlined. The extreme values of the core radius. in that region are 3475.7 and 3478.8. It was shown that the solution should be sought in the domain of the transformed parameters, since r_c and dv/dz are closely correlated.

Onofrash, N I., A. V. Drumya, and A. A. Roman. **Qualitative estimate of seismic effect using descriptive data.** AN Mold SSR. Izvestiya, no. 2, 1974, 80-90.

Five qualitative methods are proposed for mapping isoseismal curves. The problem was formalized by methods of: 1) information theory; 2) hypothesis verification; 3) parameter evaluation; 4) image recognition; and 5) taxonomy. The first four methods are based on use of all information contained in factual material as well as prior information and intensity scale. The last method is based exclusively on factual material. The methods are illustrated by examples.

Bardan, V. Seismic trace resampling. Studii si cercetari de geologie, geofizica, geografie. Geofizica, v. 12, 1974, 97-106.

In the digital recording of seismic data, the sampling interval is 1, 2, 4 or 8 msec, depending upon the highest frequency of the seismic signal. Often, to increase the speed of data processing, a changing of the sampling rate is used (for instance from 2 msec to 4 msec). This paper is an attempt to present the resampling theory of seismic data.

In the first part of the article sampling theory and aliasing phenomenon are presented. The method for resampling the seismic trace with a different interval is the content of the second part. The design of a digital minimum phase antialiasing filter is presented in the last part.

Iosif, T., and S. Iosif. Optimization of seismic station distribution in Rumania. Studii si cercetari de geologie, geofizica, geografie. Geofizica, v. 12, 1974, 51-88.

In order to analyze the distribution of the seismic stations in Romania, standard errors of the earthquakes parameters (origin time and focus position) for that territory have been calculated. The values of the standard errors depend on the spatial distribution of the seismic stations and can, therefore, be used to make quantitative comparison among different distributions of the stations.

Nine combinations of stations, including the existing network and proposed locations for new seismic stations, are described (see Fig. 1 and Table 1). If the locations of new seismic stations are properly chosen, the accuracy in determing focal parameters improves significantly. The calculations used for the study are based on the Monte Carlo method.

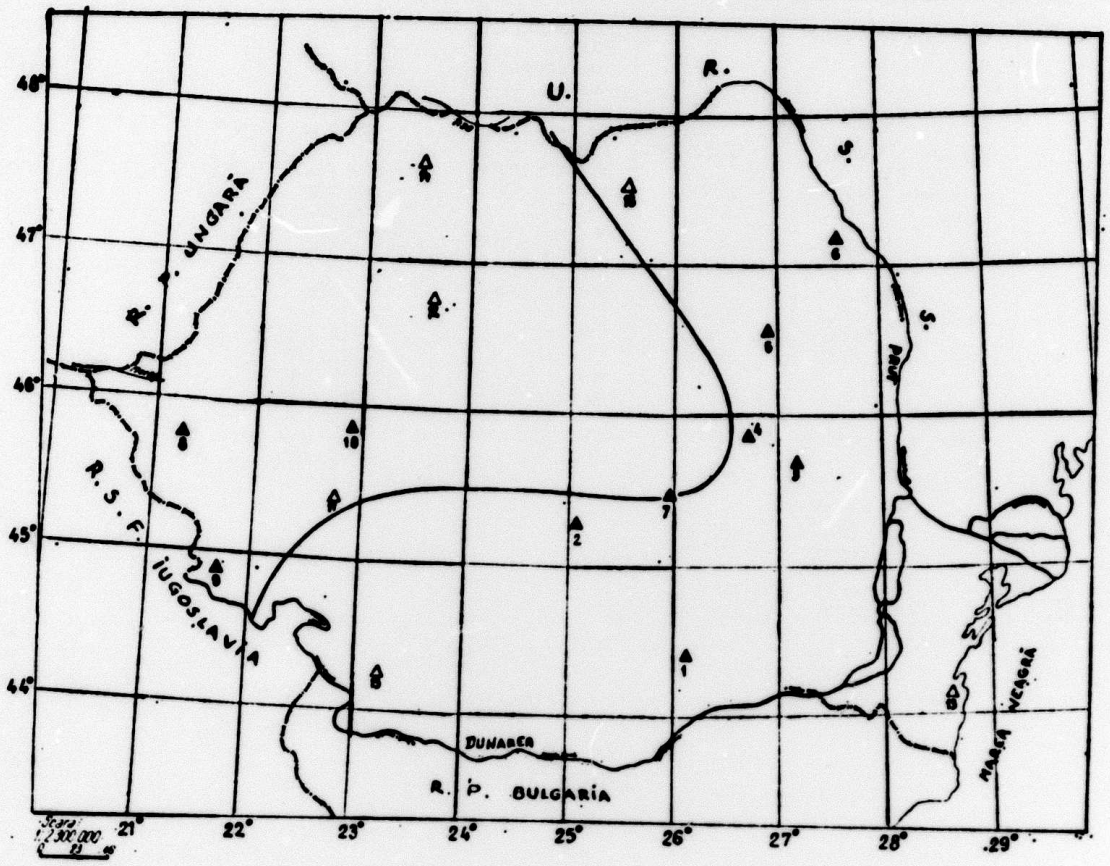

Fig. 1. Present Rumanian Seismic Network (▲) and Proposed Stations (△). The station numbers correspond to those given in Table 1.

No.	Station	Coordinates		Instrument	
		°N	°E		
1.	Bucureşti	44°24,8′	26°05,8′	Galitzin	– NS, EW
				Kirnos	– Z
				Mecanic 540 kg	– NS, EW
				450 kg	– NS
2.	Cîmpulung	45°16,1′	25°02,3′	Hiller	– NS, EW, Z
				Mecanic 150 kg	– NS, EW
3.	Focşani	45°41,7′	27°11,0′	Hiller	– Z
				Mecanic 150 kg	– NS, EW
4.	Vrîncioaia	45°52,2′	26°13,5′	VEGIK	– NS, EW, Z
5.	Bacău	46°31′	26°54′	VEGIK	– NS, EW, Z
				Mecanic 105 kg	– NS, EW
6.	Iaşi	47°11,1′	27°33,7′	VEGIK	– NS, EW, Z
				Kirnos	– Z
				Mecanic 150 kg	– NS, EW
7.	Cheia	45°28′	25°57′		
		45°53′	22°55′	VEGIK	– NS, EW, Z
8.	Timişoara	45°15,0′	21°13,5′	VEGIK	– NS, EW, Z
				Kirnos	– NS, EW, Z
				Mecanic 450 kg	– NS, EW
				200 kg	– NS, EW
9.	Sasca	41°53′	21°42′	VEGIK	– NS, EW, Z
10.	Deva			SKM	– NS, EW, Z
11.	Gura Zlata	45°,4	22,8		
	Aditionale				
12.		46°45′	23°39′		
13.		41°12′	28°38′		
14.		47°40′	23°30		
15.		44°15′	23°15′		
16.		47°32′	25°33′		

Table 1. Rumanian Seismic Stations.

Malischewsky, P. The influence of curved discontinuities on the propagation of seismic surface waves (In English). Gerlands beitrage zur geophysik, v. 83, no. 5, 1974, 355-362.

The interaction of seismic surface waves with curved discontinuities is considered. This is realized for the first time on the basis of Alsop's method by using a curvilinear co-ordinate system. The obtained reflection and transmission coefficients are complex; that means, the corresponding phase shifts of seismic surface waves at curved discontinuities can be different from 0 or π.

Bisztricsany, E., and Gy. Szeidovitz. Strain seismograph (In English). Acta geodaetica, geophysica et montanistica, v. 8, nos. 3-4, 1973, 483-488.

At the Budapest Seismological Observatory the first Hungarian strain-seismometer has been built. The 22 m long strainmeter has been constructed from 55 porcelain rods of 65 mm diameter, thus its cost is rather low. The thermal expansion coefficient of the porcelain used is not much greater than that of the quartz.

Guterch, A. Refraction studies of structure of the Earth's crust and upper mantle with deep seismic sounding method on the territory of Poland (In English). Acta geophysica Polonica, v. 22, no. 3, 1974, 225-246.

The paper presents consecutive stages and major results of investigations of the earth's crust and upper mantle made with the deep seismic sounding method in Poland in the years 1961-1973. Basic properties of the deep crustal structure have been determined along the SW-NE direction intersecting the main tectonic units of Poland. Numerous deep fractures were found to occur; they are of great importance in the tectonics of Poland, in particular in the problem of determining the margin of the pre-Cambrian platform of Eastern Europe, which is one of the major tectonic problems in Europe. The structure and physical properties of the transition zone between the crust and upper mantle have been determined in the fore-Sudetic region and the zone of the Teisseyre-Tornquist line.

Chen Pei-shau and Yen Shou-min. **Relation between seismic source mechanism and intensity distribution (In Chinese).** Acta geophysica Sinica, v. 18, no. 1, 1975, 11-25.

In this paper, the authors combine the Haskell's model which is a moving fault of finite length and the Aki's so-called ω^2 model which is constructed by fitting an exponentially decaying function to the autocorrelation function of the dislocation velocity. Neglecting some secondary factors and terms and at the same time considering its relation to earthquake intensity, the authors have troposed a model for computing the distribution of earthquake intensity. Using this model and the seismic source parameters obtained by source mechanism studies, the authors computed the theorectical distributions of earthquake intensity for four typical earthquakes. Comparison of the theoretical with the observed distributions shows the agreement is close. It shows that this model not only can explain many earthquake intensity distributions in practice, some of which are hard to explain from the point of view of geological structures, but also may be used for computing the theoretical earthquake intensity distribution for a very large area.

Kao Lung-shen, and Ge Huan-chen. **A preliminary study of P- and S-wave velocities under high pressure for rock samples from the mainland of China (In Chinese).** Acta geophysica Sinica, v. 18, no. 1, 1975, 26-38.

The compressional (P) and transversal (S) wave velocities of 20 specimens of 10 different rock types and 1 specimen of silver chloride were determined under high pressure. The pressure in measuring the P-wave velocity of three of the specimens went up as high as 20,000 kg/cm^2. It was found that above 4,000 kg/cm^2 of pressure, the change of velocity with pressure became practically linear, but the rate of change decreased gradually when the pressure was greater than 10,000 kg/cm^2.

For the determination of the S-wave velocity, in order to obtain more accurate first arrival times, coupled circuits were connected respectively to both the emitting and receiving crystals. By employing a method of "extrapolation of multiple points" measurement of the S-wave train, we can reasonably raise the accuracy. Errors of the results were then analysed.

Liu Yi-ming, Yao Hung, and Chou Hai-ran. Analysis of the characteristics and trend of seismic activities in the Keping, rupture zone in Sinkiang, China (In Chinese). Acta geophysica Sinica, v. 18, no. 1, 1975, 39-51.

Using the results from the analysis of the Keping earthquake of 6.2 magnitude (Richter scale) in western Sinkiang in 16 January 1972, a further study of the seismic activities for a larger region around Keping is made. The characteristics of seismicity, source mechanisms, velocity variations, as well as tectonic movements of the region are correlated and analyzed. Basing upon the results obtained, a preliminary discussion of the trend of seismic activities in the region is attempted.